Independently Control over Stiffness and Extensibility of Elastomers

Zihao Gong
Qingdao, Shandong,
China

M.S. Polymer Science, University of Akron, 2017

A Thesis presented to the Graduate Faculty of the
University of Virginia in Candidacy for the Degree of
Master of Science

Department of Material Science and Engineering

University of Virginia
December, 2021 Degree **will be Conferred**

Abstract

Independently Control over Stiffness and Extensibility of Elastomers

Elastomer networks are unique compared to hard materials such as metal and ceramic due to their small stiffness, large stretchability and ability to get back to its original size and shape after deformation. Yet the stiffness and stretchability of an elastomer network are intrinsically correlated: an elastomer network with a higher stiffness is less stretchable. To achieve independent control over the stiffness and extensibility of elastomer network, we designed linear-hybrid bottlebrush-linear (LhBBL) triblock copolymers, in which end blocks are linear polymers of relatively a high glass transition temperature T_g, whereas the middle blocks consist both bottlebrush polymers of relatively a low glass transition temperature T_g and short linear polymers of relatively a high glass transition temperature T_g. We use tensile test to investigate the mechanical behavior of the LhBBL copolymers. By increasing the ratio between short linear polymers and bottlebrush polymers, the elastomers exhibit stable stiffness but increasing extensibility.

Table of content

Acknowledgement

I would like to give my deepest appreciation to my graduate advisor, Prof. Liheng Cai, for his continuous guidance and help on both my studies and life.

I wish to express my gratitude to all my groupmates who helped me a lot on my research project.

Last but not least, I would like to thank my parents for supporting me in these years and encouraging me to finish my Master Degree.

List of Figures

List of Schemes

List of Tables

Chapter I Stiffness and Extensibility of Elastomers

1.1 Basic concept of elastomer elasticity.

1.1.1 Elasticity of a single polymer chain

Long, flexible chain-like molecules make up elastomeric materials. Conventional rubbers are made up of large molecular weight chains that can change form and flow under stress if the temperature is higher than the glass transition temperature (Tg) of the polymer. In the case of an isolated chain, Brownian motion is the motivation of the chain randomly move during chain transformation in a stress-free condition, as shown in Figure 1.1. (a). Under an external stress, the elastomeric chain can also adopt an orientated conformation, resulting in a stretched chain under the tensile stress, as shown in Figure 1.1. (b). The average end-to-end distance is r_0 when the chain is relaxed whereas it becomes r when the chain is stretched.

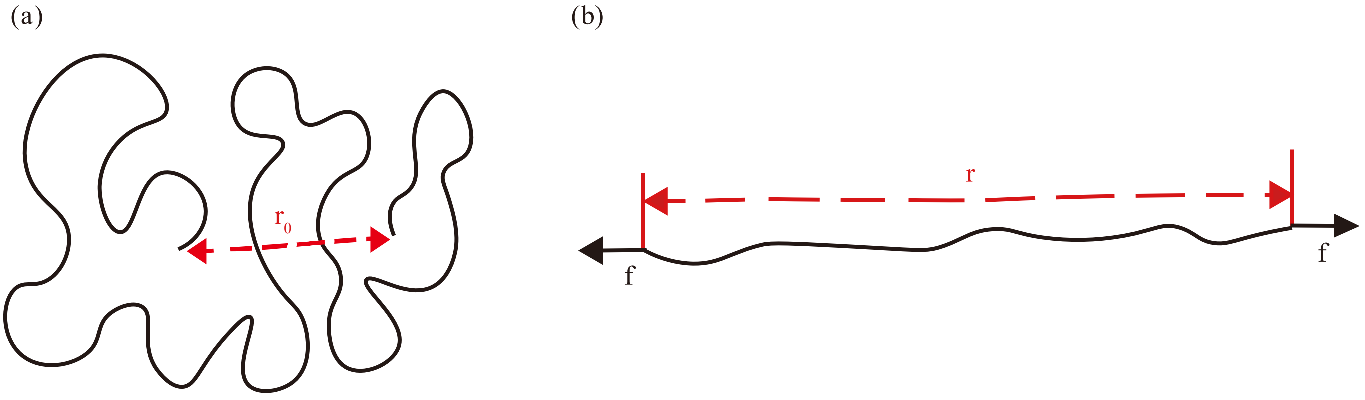

Figure 1.1: Diagram of Polymer chain, (a) A random polymer chain, and (b) A stretched polymer chain[1–4]

In an ideal chain, the energy is zero.[3] Under an external stress, an ideal chain elongates and assumes a less likely conformation resulted in a lower entropy. As a result, the elasticity is entirely entropic. According to Boltzmann, the entropy has a form of

$$S(\vec{R}) = k \ln W_N(\vec{R}) \qquad (Eq\ 1.1)$$

Where k is the Boltzmann constant, $W_N(\vec{R})$ is the number of chain conformations of a single ideal chain with the end-to-end distance $\vec{R}$.

The probability distribution for the end-to-end distance in the ideal coil $P_N(\vec{R})$ can be expressed as

$$P_N(\vec{R}) = (\frac{3}{2\pi N b^2})^{3/2} \exp\,(-\frac{3R^2}{2Nb^2}) \qquad (Eq\ 1.2)$$

$$R \sim \sqrt{< R^2 >} = N^{1/2} b \qquad (Eq\ 1.3)$$

$$L = Nb \qquad (Eq\ 1.4)$$

In which, L is the contour length of the polymer chain, N is the number of Kuhn segments, b is the Kuhn length.

Obviously:

$$W_N(\vec{R}) = const\ \times P_N(\vec{R}) \qquad (Eq\ 1.5)$$

Therefore the entropy can be expressed by contour length and Kuhn length with form of

$$S(\vec{R}) = -\frac{3kR^2}{2Lb} + const \qquad (Eq\ 1.6)$$

And for the free energy

$$F = E - TS = -TS = \frac{3kTR^2}{2Lb} + const \qquad (Eq\ 1.7)$$

Finally, the force is the derivative of the free energy with respect to R:

$$\vec{f} = \frac{\partial F}{\partial \vec{R}} = \frac{3kT}{Lb}\vec{R} \qquad (Eq\ 1.8)$$

The polymer chain elongates along the direction of the external force and the elongation follows the Hook's law which is proportional to the force. The coefficient $\frac{3kT}{Lb}$ is the elastic modulus $(Eq\ 1.9)$ which is inversely proportional to the contour length L, and thus is smaller for longer chains. The elastic modulus is also proportional to kT which indicates the entropic nature of high elasticity. The conclusion is that long polymer chains are susceptible to external stress.

$$E = \frac{3kT}{Lb} \qquad (Eq\ 1.9)$$

1.1.2 Elasticity of polymer networks

A polymer network is made up of long polymer chains that are crosslinked to generate a large three-dimensional macromolecule as shown in Figure 1.2. Except for those in the glassy or partially crystalline conformations, all polymer networks have great elasticity.[1–3] The polymer networks are unique due to their ability to undergo substantial reversible deformations under a relatively low applied stress. High elasticity is the most distinguishing attribute of polymer materials, and it is connected to the most fundamental characteristics of ideal chains.[5,6] Rubbers are extremely elastic polymer compounds that are commonly used in daily life. Rubber's elasticity is made up of the elastic responses of the crosslinked chains in the network sample.[6] External stress alters a chain's end-to-end distance at equilibrium state, causing it to adopt a less likely conformation. As a result, rubber's elasticity is essentially entropic nature.[2,3]

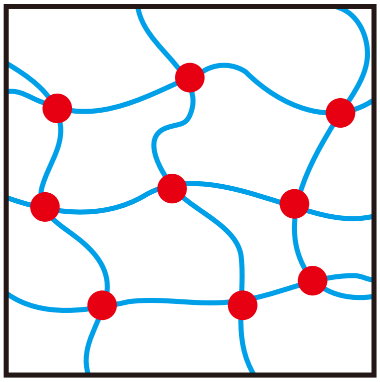

Figure 1.2: Polymer network (red dots: crosslinkers; blue lines: network strands)

There are several constitutive models based on different assumptions to describe the physical behavior of the conformation of a single chain and the behavior of the strands in the network.[3] In this section, we'll go over the relevant models I used in our research in further depth: Affine network model and Phantom network model.

1.1.2.1 Affine network model

The affine network model, first proposed by Kuhn, is the simplest model that encapsulates the concept of rubber elasticity. The affine network model's primary assumption is that each network strand's relative deformation is the same as the macroscopic relative deformation imposed on the entire network.[2,3] Moreover, the end of each identical network strands is permanently fixed at the nonfluctuating background.[6]

Consider a system of crosslinked chains that are densely packed as shown in figure 1.3. Assume free-jointed chains with segment lengths of l and contour lengths of L. The network has undeformed dimensions L_{x0}, L_{y0}, L_{z0}. Let the network undergoes relative deformations in three directions by factors of $\lambda_x, \lambda_y, \lambda_z$ respectively, then the dimensions of the deformed network are

$$L_x = \lambda_x L_{x0}, L_y = \lambda_y L_{y0}, L_z = \lambda_z L_{z0} \qquad (Eq\ 1.10)$$

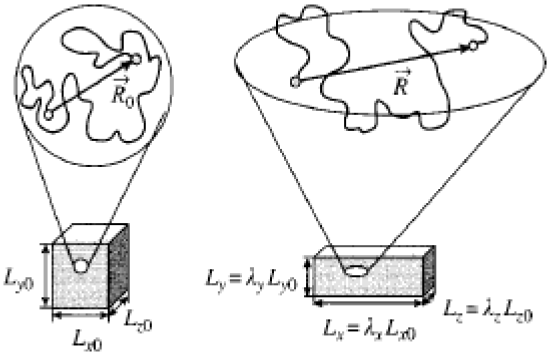

Figure 1.3 Schematic diagram of the Affine network model.[3]

As illustrated in Figure 1.3, the end-to-end vector of one network strand is $\overrightarrow{R_0}$, and the projections along three axes are $\overrightarrow{R_{x0}}, \overrightarrow{R_{y0}}, \overrightarrow{R_{z0}}$, respectively before deformation. In the Affine assumption, each network strand has the same deformation as the whole polymer network. Thus, the end-to-end vector of a such network strand is $\vec{R}$ after deformation and the projections along three axes are

$$\overrightarrow{R_x} = \lambda_x \overrightarrow{R_{x0}}, \overrightarrow{R_y} = \lambda_y \overrightarrow{R_{y0}}, \overrightarrow{R_z} = \lambda_z \overrightarrow{R_{z0}} \qquad (Eq\ 1.11)$$

Recall the entropy of a polymer chain (Eq 1.6)

$$S(\vec{R}) = -\frac{3kR^2}{2Nb^2} + const = -\frac{3k}{2Nb^2}(R_x^2 + R_y^2 + R_z^2) + const \qquad (Eq\ 1.12)$$

The entropy change from deformed stated to undeformed states is

$$\Delta S = S(\vec{R}) - S(\overrightarrow{R_0}) = -\frac{3k}{2Nb^2}\left(R_x^2 + R_y^2 + R_z^2\right) + \frac{3k}{2Nb^2}\left(R_{x0}^2 + R_{y0}^2 + R_{z0}^2\right)$$

$$= -\frac{3k}{2Nb^2}\left[(\lambda_x^2 - 1)R_{x0}^2 + \left(\lambda_y^2 - 1\right)R_{y0}^2 + (\lambda_z^2 - 1)R_{z0}^2\right] \qquad (Eq\ 1.13)$$

The entropy change of the whole network with n network strands is the summation of all network's n strands

$$\Delta S_{net} = -\frac{3k}{2Nb^2}\left[(\lambda_x^2 - 1)\sum_{i=1}^{n} R_{x0i}^2 + \left(\lambda_y^2 - 1\right)\sum_{i=1}^{n} R_{y0}^2 i + (\lambda_z^2 - 1)\sum_{i=1}^{n} R_{z0i}^2\right] \qquad (Eq\ 1.14)$$

Assume the network is in ideal state, then the summations of the squares of the end-to-end vector on three axes can be expressed by

$$\sum_{i=1}^{n} R_{x0i}^2 = \sum_{i=1}^{n} R_{y0i}^2 = \sum_{i=1}^{n} R_{z0i}^2 = \frac{nNb^2}{3} \qquad (Eq\ 1.15)$$

Substitute the Eq 1.15 into Eq 1.14, I can simplify the entropy change of the whole network with only strands number n, Boltzmann constant k and deformation factors:

$$\Delta S_{net} = -\frac{nk}{2}\left(\lambda_x^2 + \lambda_y^2 + \lambda_z^2 - 3\right) \qquad (Eq\ 1.16)$$

Combine the Eq 1.7 and Eq 1.16, the free energy needed for the deformation is

$$\Delta F_{net} = -T\Delta S_{net} = \frac{nkT}{2}\left(\lambda_x^2 + \lambda_y^2 + \lambda_z^2 - 3\right) \qquad (Eq\ 1.17)$$

From the above equation, notably, the free energy required for network deformation is independent of contour length L, Kuhn length b, or number of Kuhn monomer N, the parameters which describe the identical sub polymer chains. This demonstrates that the Affine model theory is universal, it is unaffected by neither the microscopic specifics of chain flexibility, nor the values of subchain's contour length and Kuhn segments, nor the specific structure of the molecular mass distribution.

If I apply the theory to the case of uniaxial deformation, assume the network is either stretched or compressed in a single direction, say along x axis. Since the polymer network is incompressible, the volume of the network does not vary appreciably during deformation. In this case, the product of deformation factors is unity to keep the volume remain stable.

$$\lambda_x \lambda_y \lambda_z = 1 \qquad (Eq\ 1.18)$$

For uniaxial deformation,

$$\lambda_x = \lambda \quad \lambda_y = \lambda_z = 1/\sqrt{\lambda} \qquad (Eq\ 1.19)$$

Substitute these deformation factors into Eq 1.17, I can get the free energy change required for a uniaxial deformation:

$$\Delta F_{net} = \frac{nkT}{2}\left(\lambda^2 + \frac{2}{\lambda} - 3\right) \qquad (Eq\ 1.20)$$

The force needed to deform the network along x axis is the derivative of the free energy with respect of the length along x axis:

$$f_x = \frac{\partial \Delta F_{net}}{\partial L_x} = \frac{\partial \Delta F_{net}}{\partial (\lambda L_{x0})} = \frac{nkT}{L_{x0}}\left(\lambda - \frac{1}{\lambda^2}\right) \qquad (Eq\ 1.21)$$

Furthermore, the stress along x axis is the ratio between the force along x axis f_x to the cross-section area $L_y L_z$,

$$\sigma_x = \frac{f_x}{L_y L_z} = \frac{nkT}{L_y L_z L_{x0}}\left(\lambda - \frac{1}{\lambda^2}\right) = \frac{nkT}{V}\left(\lambda^2 - \frac{1}{\lambda}\right) \qquad (Eq\ 1.22)$$

Here $V = L_{y0} L_{z0} L_{x0}$ is the initial volume of the polymer network. If the stress remain constant and temperature T increases, the value of deformation factor λ will decrease. That is the reason why rubbers shrink during heating, contrary to crystalline material and gases.

The coefficient relating the stress and deformation factor is the shear modulus

$$G = \frac{nkT}{V} = \nu kT = \frac{\rho RT}{M_s} \qquad (Eq\ 1.23)$$

Here, n is the number of network strands, k is Boltzmann constant, T is temperature, V is the volume of polymer network, $\nu = n/V$ is the number of network strands per unit network volume, ρ is the density of polymer network, R is the gas constant, M_s is the number-average molecular weight of network strands. The network modulus increases with temperature, also increases with the number density of network strands. In one word, the network modulus is kT per strand according to Eq 1.23.

The basic assumption of affine network model is that the ends of network strands are pinned to an elastic nonfluctuating background and shift affinely with the entire polymer network as shown in Figure 1.4(a).[3,5,6]

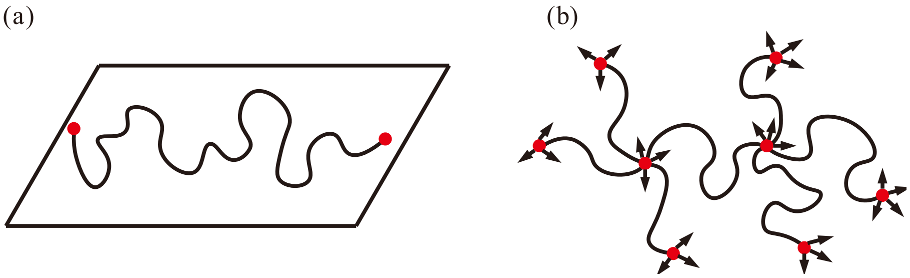

Figure 1.4 Schematic diagram of polymer network model: (a) Affine network model; (b) Phantom network model[2,3]

1.1.2.2 Phantom network model

In real networks, the ends of network strands are connected to other strands. Those crosslink junctions are not permanent in space and their positions can shift around their averages.[3,5,6] By decreasing the cumulative extension of the network strands, these movements result in a net reduction in the system free energy. To incorporate such movements, the Phantom network model has been used.[3] In a phantom network model, unlike the affine network model, the strands are ideal chains with ends of strands linked at fluctuating crosslink junctions as shown in Figure 1.4(b).[3] According to the phantom network model, crosslink junctions in the bulk movement about their average position. The macroscopic deformation of the network, which refers to the deformation of single polymer chains, is determined by the degree of the fluctuations.

To obtain the expression of phantom network model, I need to introduce an idea of fluctuations of effective chains.[3,6,7] Consider an ideal chain with fixed ends, the fluctuations of a single monomer within such ideal chain are equivalent to that of an end monomer in a single effective chain with K monomers. In the case of the center monomer of an ideal chain of $2N$ monomers, the effective chain has $K = N/2$ monomers. As a result, the confining effect of the two N monomer strands is the same as that of a single effective chain of $K = N/2$ monomers. In general, the fluctuations of a branch point in an f-arm star polymer are identical to the fluctuations of an effective chain with monomer number of

$$K = \frac{N}{f} \qquad (Eq\ 1.24)$$

The situation of crosslink junction in phantom network is similar to that of the branch point of an f-arm star polymer. In phantom network model, one end of a network strand is attached to the elastic nonfluctuating background, which is called seniority-zero strands. Then $f - 1$ strands attach with that end point. Each seniority-zero strands are connected to a single seniority-one strand by an f-functional crosslink. Those $f-1$ seniority-zero strands can be substituted with a single effective chain comprising N_1 monomers, which has the same restricting effect as the original $f-1$ chains combined:

$$N_1 = \frac{N}{f-1} \qquad (Eq\ 1.25)$$

The single effective chain with N_1 monomers is linked in series with a single seniority-one N-mer and together they form an effective chain with monomer number of:

$$K_1 = N + N_1 = N(1 + \frac{1}{f-1}) \qquad (Eq\ 1.26)$$

Furthermore, the $f-1$ of the seniority-one network strands are linked at a single crosslinker to one seniority-two strand. The effective chains of these seniority-one strands can be substituted by the effective chain with number of monomers:

$$N_2 = \frac{K_1}{f-1} = N[\frac{1}{f-1} + \frac{1}{(f-1)^2}] \qquad (Eq\ 1.27)$$

Thus, the effective chain corresponding the effect of all strands from seniority-zero to seniority-two has monomers of:

$$K_2 = N + N_2 = N[1 + \frac{1}{f-1} + \frac{1}{(f-1)^2}] \qquad (Eq\ 1.28)$$

Continuing with this procedure yields the number K of monomers in an effective chain which represents the entire effect of all network strands within the phantom network:

$$K = N\left[1 + \frac{1}{f-1} + \frac{1}{(f-1)^2} + \frac{1}{(f-1)^3} + \cdots\right] = \frac{N}{1 - 1/(f-1)}$$

$$= \frac{f-1}{f-2}N \qquad (Eq\ 1.29)$$

This equation indicates that an effective chain with K monomers can replace each of the initial $f-1$ chain. The elastic nonfluctuating background is connected to the end of each network strand by this effective chain. Each network strand has $f-1$ of these effective chains, which can be substituted by another effective chain with monomers of

$$\frac{K}{f-1} = \frac{N}{f-1} \qquad (Eq\ 1.30)$$

Each network strand contains one of these effective chain on its end. I can use one combined chain to represent an N-monomers network strands with two $N/(f-2)$-monomers effective chains. This combined chain has a number of monomers of:

$$N_{combine} = N + \frac{2N}{f-2} = \frac{f}{f-2}N \qquad (Eq\ 1.31)$$

In phantom network model, the shear modulus can be obtained by replacing N with $N_{combine}$ from the Eq 1.23 of affine network model:

$$G = \nu kT\frac{f-2}{f} = \frac{\rho RT}{M_s}(1 - 2/f) \qquad (Eq\ 1.32)$$

In conclusion, both affine network model and phantom network model are based on an flexible network. The front facto is the only variation between these two models. According to several studies, the phantom network model is more accurate than the other one.[7,8] As a result, the phantom network model becomes the foundation for subsequent research in polymer network elasticity theory.

1.2 Mechanical behavior of polymers

1.2.1 Stress-strain behavior of polymers

A material specimen is subjected to a tension or compression test to assess the connection between stress and strain. In this test, a test specimen is subjected to a continually growing axial force, and the deformation is measured as the load increases. A load-deformation curve can be plotted using these data. The test specimen's deflection is determined by the material's elastic modulus as well as the specimen's shape (area and length). Because scientists are more cared about mechanical behavior rather than geometry of the material, it's helpful to generalize the data to eliminate the effect of geometry. This is accomplished by converting load values to stress values and deflection values to strain values as follows:

$$\sigma = \frac{P}{A_0};\ \varepsilon = \frac{L - L_0}{L_0} = \frac{\delta}{L_0} \qquad (Eq\ 1.33)$$

In the above equation, σ is the stress, P is the load, A_0 is the initial cross-sectional area of the specimen, ε is the strain, L is the current length of the test specimen, L_0 is the initial length of the specimen.

A stress-strain curve can be drawn using the stress and strain data obtained from the tensile test, as shown in Figure 1.5. The stress-strain curve reveals many mechanical behavior of the material. **P** is the proportionality limit, or maximum value of stress at which the stress-strain curve is linear; **E** is the elastic limit, which is the highest stress value at which no permanent set exists; **Y** is the yield point, which is the stress value over which the strain begins to quickly grow; **U** corresponds to the ultimate strength also known as the tensile strength; F is the fracture point or break point at which the sample break and splits into two pieces. In practical, scientist usually use Young's modulus (*E*) which is the slope of the curve before elastic limit to describe the stiffness of the material and use elongation at break (ε_{break}) to describe the stretchability of the material.

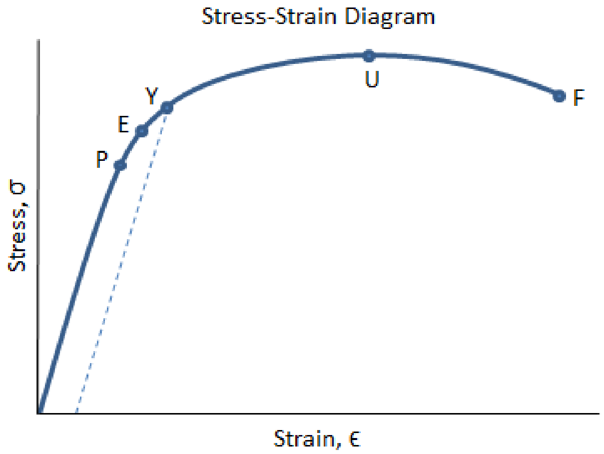

Figure 1.5 A typical stress-strain curve

Brittle plastic, tough plastic, and elastomer are the three basic types of polymeric materials with different behaviors. Brittle polymers exhibit elastic moduli of a few GPa and a linear stress-strain curve with a modest distortion up to the fracture point (Figure 1.5(a)). Polymers that exhibit this property are usually glassy at ambient temperature or have a high glass transition temperature (T_g), such as poly(methyl methacrylate), polystyrene, and poly(acrylic acid).[9,10]

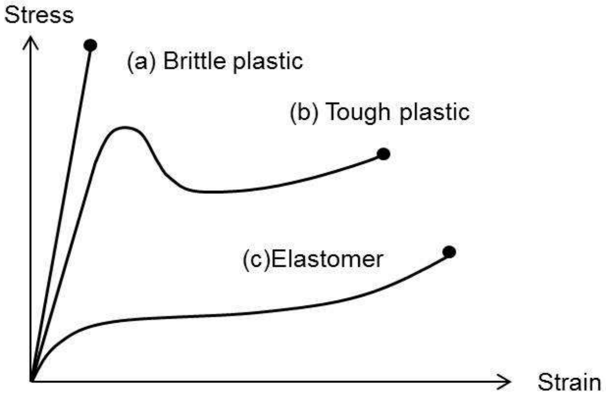

Figure 1.6 Stress-strain curve of polymeric materials.[11]

The glassy polymers have a tough plastic behavior. Such behavior is common in semi-crystalline polymers with an amorphous fraction above the T_g, such as polyethylene, polytetrafluoroethylene, polyethylene terephthalate, polyamide(Figure 1.5(b)). These polymers have a lower initial modulus or Young's modulus than brittle plastics. A yield point is seen on the stress-strain curve, which is followed by significant elongation and, in some cases, necking.

The Young’s modulus of an elastomer is typical in the MPa range, the stress-strain curve is substantially non-linear, and deformation is generally reversible up to several hundred percent elongations at break (Figure 1.5(c)). Many elastomers, such as silicone rubber, natural rubber, , styrene-butadiene rubber, exhibit this type of behavior.

1.2.2 Intrinsic correlation between stiffness and extensibility of polymer network

Commercial silicone elastomers are frequently employed in soft material research because of their unique mechanical properties, including extremely soft stiffness (kPa-MPa), large stretchability (several hundred percent elongation at fracture), reversibility after deformation, and easily tunable mechanical properties. Two main characteristic properties are stiffness and extensibility which can be identify simultaneously using stress-strain curve. Scientists extract the Young’s modulus from the slope of the elastic regime to describe the stiffness whereas use the elongation at fracture to indicate the extensibility of the material. Unfortunately, the intrinsic correlation between these two mechanical parameters limits the understanding of the elastomer physics and the application of elastomers. Figure 1.7 shows a stress-strain curve of a general commercial silicone elastomer, Sylgard 184 with different mixing ratio between silicone base and crosslinking agent.[12] With the increasing of crosslinking agent, the elastomer becomes stiffer but less stretchable.

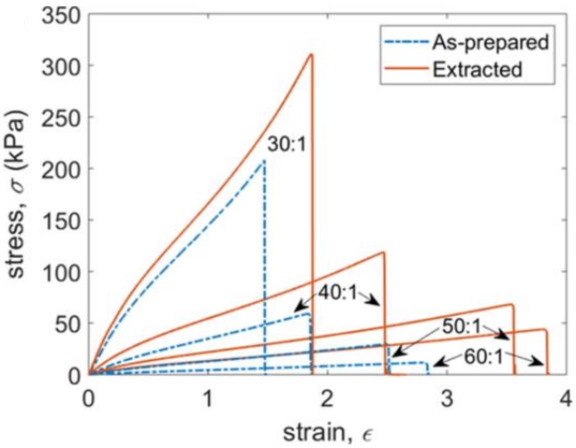

Figure 1.7 Stress-strain curve of Sylgard 184 with different mixing ratio (silicone base: crosslinking agent= 30:1, 40:1, 50:1, 60:1)[12]

The reason is easily understanding when I express the stiffness and extensibility of elastomer networks with their structural parameters.[2,3] From Eq 1.23 and Eq 1.32, I can express the Young's modulus:

$$E = 2G(1+\upsilon) = \frac{3nkT}{V} = 3\nu kT = \frac{3\rho RT}{M_s} = \frac{3\rho RT}{Nm} \qquad (Eq\ 1.34)$$

Here, υ is Poisson's ratio which is about 0.5 for rubber,[8] n is the number of network strands, k is Boltzmann constant, T is temperature, V is the volume of polymer network, $\nu = n/V$ is the number of network strands per unit network volume, ρ is the density of polymer network, R is the gas constant, M_s is the number-average molecular weight of network strands, N is the number of monomers within the network strand, m is the molecular weight of a monomer. At a constant temperature and same monomer species, the stiffness is only varied by the number of monomers per network strand

$$E \approx N^{-1} \qquad (Eq\ 1.35)$$

As for the extensibility, it describe the ability of the elastomer network been deformed before breaking. In the case of uniaxial deformation, the elongation at break is[13]

$$\varepsilon_{break} = \frac{L}{R} - 1 = \frac{bN}{bN^{\frac{1}{D}}} - 1 = N^{1-\frac{1}{D}} - 1 \approx N^{1-\frac{1}{D}} \qquad (Eq\ 1.36)$$

In which L is the contour length of the network strand, R is the end-to-end distance of network strand, b is the distance between two neighboring monomers, N is the number of monomers within the network strand, D is fractal dimension of the network strand which depends on the shape of the polymer chain which is always larger than 1 (D is 2 for ideal chain for example,).

From Eq 1.34-1.36, both stiffness and extensibility of polymer network are only dependent on number of monomer at a constant temperature. That is why for a polymer system with less monomers, it will become stiffer but less stretchable. This intrinsic correlation limits the application of elastomer networks. This work aims to control the stiffness and extensibility of polymer network independently.

1.3 Molecular design

In a previous work of our group, we synthesized a linear-bottlebrush-linear (LBBL) triblock copolymer as shown in Figure 1.8 (a). We use TEM and GISAXS to characterize the microstructure of the LBBL copolymer and found it self-assembled into a random sphere network structure at room temperature.

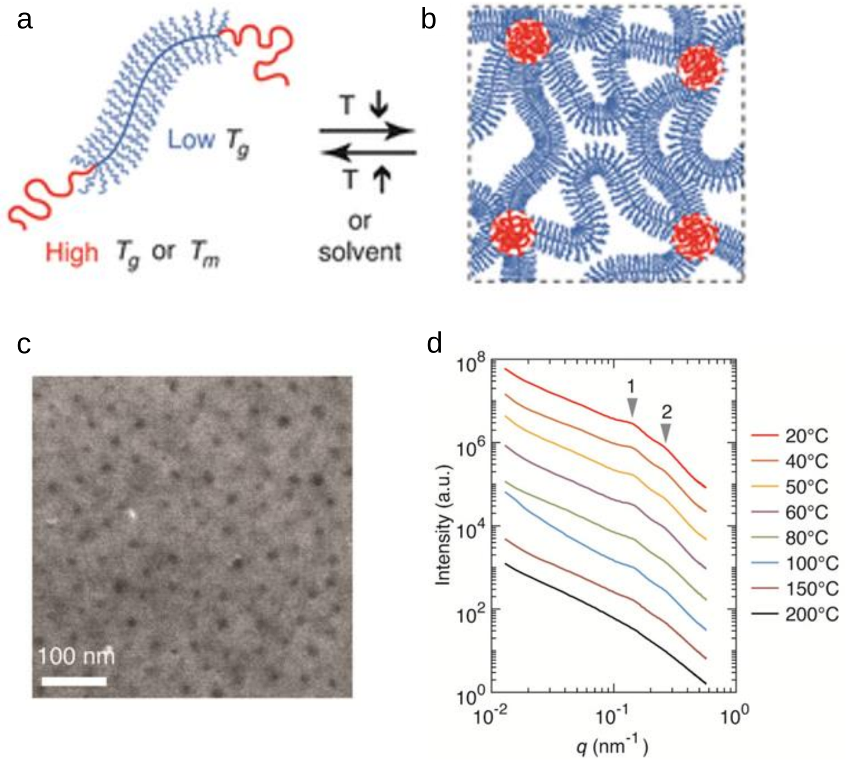

Figure 1.8 Self-assemble behavior of linear-bottlebrush-linear (LBBL) triblock copolymer. (a) Schematic of a linear-bottlebrush-linear triblock copolymer. (b) At low temperature, the LBBL copolymer self-assembles into a network structure. (c) TEM image of the elastomer. (d) *In situ* GISAXS measurements for sample reveals a random sphere structure.[14]

We seek to independently control the stiffness and extensibility of elastomers by exploiting the self-assembly of an architecturally designed bottlebrush-based ABA triblock copolymer similar to LBBL copolymer. The A blocks are a linear polymer of relatively a high glass transition temperature T_g, whereas the B block is a bottlebrush polymer with a linear backbone densely grafted by linear side chains of relatively a low T_g. Moreover, two neighboring side chains are spaced by a short linear polymer segment of a relatively high T_g; this results in a *hybrid* bottlebrush consisting of both low and high T_g polymers, as illustrated in Figure 1.8(a). In a nanostructure self-assembled by such a linear-*hybrid* bottlebrush-linear (LhBBL) triblock copolymers, the high T_g blocks can form 'hard,' glassy domains that effectively crosslink the soft, elastomeric bottlebrush domains (Figure. 1.8(b)); this forms a network reminiscent to classical thermoplastic elastomers such as poly(styrene-butadiene-styrene) (SBS). Unlike SBS in which linear polymers are entangled, for LhBBL polymers the bottlebrush architecture can prevent the formation of entanglements, enabling elastomers with extreme softness. Furthermore, at relatively low temperature, the short, high T_g spacer segments between neighboring side chains can fold to nanoscale domains. Upon extension, the folded domains unzip, enabling an exceptional extensibility as shown in Figure 1.8(c). Due to the large size difference between brush monomers and spacer monomers, the volume of the spacers can ignored compared with that of side-chains, hence the volume of network strand is only dependent on the number of brush monomers which means the stiffness of the network is controlled by the number of brush monomers. Whereas the extensibility of the network depends on the total number of space monomers and brush monomers. Consequently, exploiting the bottlebrush architecture will enable control over stiffness, whereas exploiting the spacer segments will enable control over extensibility.

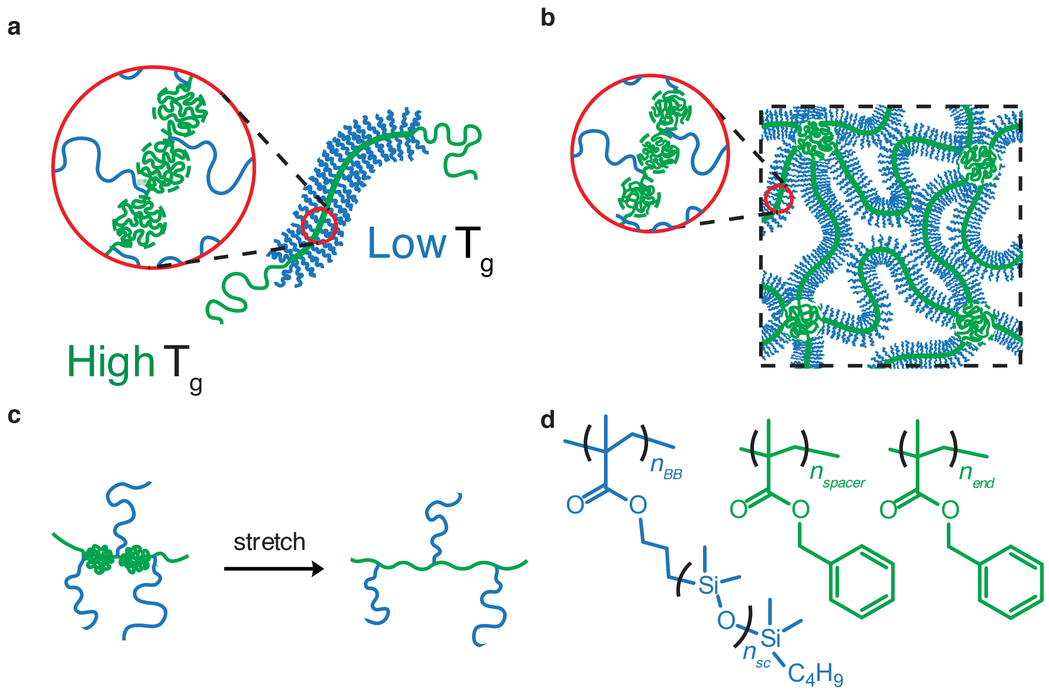

Figure 1.9 Molecular design of linear-*hybrid* bottlebrush-linear (LhBBL) triblock copolymers. (a) Molecular structure of LhBBL copolymers. (b) Self-assembled microstructure of the network formed by LhBBL copolymer. (c) Diagram of the network strand been stretched. (d) Monomer species chosen for LhBBL copolymer.

To demonstrate this concept, I choose polydimethylsiloxane (PDMS) as side-chains and poly (benzyl methacrylate) (PBzMA) as end blocks and spacers to synthesize a linear-hybrid bottlebrush-linear triblock copolymer, in which n_{BB} is the number of PDMS side chains per middle block, n_{spacer} is the number of BzMA spacers per middle block and n_{end} is the number of BzMA on each end block as shown in Figure 1.8(d). There are two reasons for us to choose PDMS and PBzMA. First, PDMS has a low T_g, about -125 °C,[15] whereas PBzMA has a T_g, about 60 °C,[16,17] the large difference between T_g of PDMS and PBzMA ensures that the self-assembled elastomer is thermally stable within a wide range of temperature. Second, PDMS and PBzMA are highly incompatible with a large Flory-Huggins interaction parameter of 0.54[16] such that microphase separation of the triblock copolymer easily falls into the strong segregation limit. Compared to the weak segregation limit, within the strong segregation limit the microstructure is much more stable and less sensitive to processing fluctuations, enabling controllable macroscopic properties.

Chapter II Controlled Radical Polymerization

2.1 Controlled radical polymerization

One of the most prevalent and practical ways for creating standard polymers is free radical polymerization (FRP).[18–20] FRP is an extremely durable and cost-effective process that accounts for a substantial amount of polymer manufacturing because of its high tolerance to material and operational imperfections, as well as its high compatibility with a wide range of monomers. Processes of FRP can be broken down into following steps, as depicted in Scheme 2.1,[18–20] namely initiator decomposition, initiation, propagation, and termination which includes both combination or disproportionation.[18–20]

Initiator dissociation: $I \xrightarrow{k_d} 2R\cdot$

Initiation: $R\cdot + M \xrightarrow{k_1} P_1\cdot$

Propagation: $P_n\cdot + M \xrightarrow{k_p} P_{n+1}\cdot$

Termination by combination: $P_m\cdot + P_n\cdot \xrightarrow{k_{tc}} D_{m+n}$

Termination by disproportionation: $P_n\cdot + M \xrightarrow{k_{td}} D_n + D_m$

Scheme 2.1 Mechanism for free radical polymerization (FRP)

In polymer chemistry, controlling polymer chain length and dispersity is crucial. The ability to precisely tune the physical properties of materials and construct macromolecules with complex microstructures is enabled by the synthesis of polymers with predetermined molecular weight (MW), low dispersity (Đ), and retained chain end functions.[18–20]

Due to the strong reactivity of intermittent radical species, inevitable termination and transfer reactions limit the lifetimes of polymer chains which will result in a broad molecular weight dispersion and undesirable polymer structure. This impedes creating more complicated and defined structures, which are necessary for advanced applications. Several methods of controlled radical polymerization (CRP) have been introduced in the last few decades. Those methods enable for far more control over polymer microstructures. CRP approaches that have been investigated the most are stable free methods. Atom transfer radical polymerization (ATRP),[21,22] nitroxide mediated polymerization (NMP),[23] and reversible addition-fragmentation chain transfer polymerization (RAFT)[21,24] are the most investigated CRP methods. The basic goal of all these polymerizations is to prevent bimolecular termination by lowering the radical concentration during the polymerization process. This is achieved by striking a balance between dormant polymer chains with mediating species and active polymer chains which are free to propagate and engage in other FRP steps as illustrated in Scheme 2.2. To inhibit termination, the equilibrium must benefit the production of dormant chains, and the formation of a dormant chain must be quick.

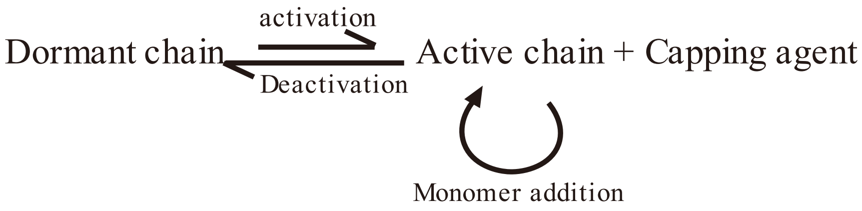

Scheme 2.2 Dynamic equilibrium in CRP

CRPs have been utilized to create polymers with a variety of chain lengths and topologies, as well as bio-polymer hybrids and block copolymers that could be applied in a variety of applications. The inclusion of diverse compositions, architectures, and functions into ATRP, for example, considerably enlarged the universe of polymers.

2.2 Atom transfer radical polymerization (ATRP)

Due to its versatility and compatibility with a wide range of monomers, ATRP is the most studied CRP technique, allowing for the synthesis of functional polymers with well-defined compositions. Sawamoto et al. and Wang and Matyjaszewski, independently discovered ATRP in 1995.[21,22] Since then, an enormous amount of research has been written on ATRP in bulk and solution, with the majority of the work utilizing copper bound to a nitrogen-based ligand as the mediating species due to copper's low cost and adaptability in comparison to other transition metals.[18,25,26]

2.2.1 Mechanism of Atom transfer radical polymerization (ATRP)

As illustrated in Scheme 2.3, ATRP enables the reversible activation or deactivation of developing radicals through a dynamic equilibrium with a transition metal complex (Mtn-Y/Ligand) and an interchange of halide atom (X) between the chain end and the metal complex,. Due to the fact that the rate coefficient for deactivation (k_{deact}) is significantly greater than the rate coefficient for activation (k_{act}), the significant fraction of chains exist in a dormant state capped with halogen (R-X), which inhibits bimolecular radical termination and enables control over the polymer structure. Additionally, inevitable radical termination results in the accumulation of deactivating species. This moves the balance toward the dormant species and further decreases the concentration of active radicals, hence preventing termination.[27,28] Additionally, rate of deactivation (k_{deact}) is comparable to that of termination (k_t), because the deactivator concentration is substantially greater than the radical concentration, deactivation becomes the dominating chain terminating process.

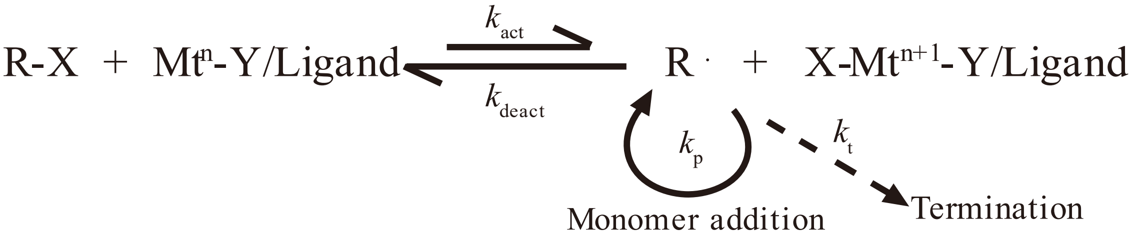

Scheme 2.3 Mechanism for ATRP.[29]

2.2.2 Components in ATRP

Generally, the ATRP system is composed of a monomer, an initiator containing a halogen atom, and a catalyst composed of metal species and ligand. Certain ATRP systems also require solvent.

2.2.2.1 Monomers

The monomer chosen dictates the initiator and catalyst to be used, as well as the temperature and solvent to be used. The polymerization of styrene, acrylonitrile, (meth)acylates, meth(acrylamides), have all been well studied through ATRP.[18–21,30,31] Additionally, ATRP is tolerant of a variety of functional groups, including epoxides, amines, and hydroxyl groups. Vinyl pyridines cannot be polymerized only if a strongly coordinating ligand is used to prevent the monomer from covalently linking to the transition metal. In contrast, acidic monomers cannot be polymerized by an ATRP system due to the ligand's protonation. However, Jana et al. recently revealed a dual functional unimolecular ligand initiator system that enables ATRP of (meth)acrylic acids.

2.2.2.2 Initiator

The initiator is responsible for determining the number of propagating chains and hence the degree of polymerization (DP).[25] Due to the quick initiation and negligible transfer and termination events, the number of propagating chains is equal to the concentration of the initial initiator; consequently, the degree of polymerization (DP) can be determined as

$$DP = \frac{[M]_0}{[I]_0} \times conversion \qquad (Eq\ 2.1)$$

In which $[M]_0$ and $[I]_0$ are the initial concentration of monomer and initiator respectively.

The initiator is often constituted of an alkyl halide, with either bromide or chloride being the most frequently used halide. The homolytic cleavage of the initiator's instable bond produces a free radical capable of initiating the polymerization. Bromide halides have a lower bond dissociation energy than chloride halides, implying that bromide halides are more efficient for initiation.

2.2.2.3 Catalyst

The catalyst is critical in ATRP because it controls the balance of active species and dormant species. The catalyst should ideally be highly selective for atom transfer and should not participate in other processes, also, deactivation should be exceedingly quick. The transition metal must have two accessible oxidation states and an affinity for the halogen atom, whereas the ligand must form a moderately strong complex with the metal. Copper is the most often used transition metal due to its inexpensive cost and compatibility with a wide variety of monomers. Numerous additional metals, including chromium, titanium, rhenium, molybdenum, osmium, ruthenium, iron, rhodium, palladium, and nickel have also been used.[32–34]

2.2.2.4 Ligands

Catalytic activity and selectivity are strongly ligand-dependent, as the ligand regulates the metal center's redox potential. Another critical function of the ligand is to increase the solubility of the metal in organic solvents. A list of ligands with the rate of both activation and deactivation is shown in Figure 2.1.[35]

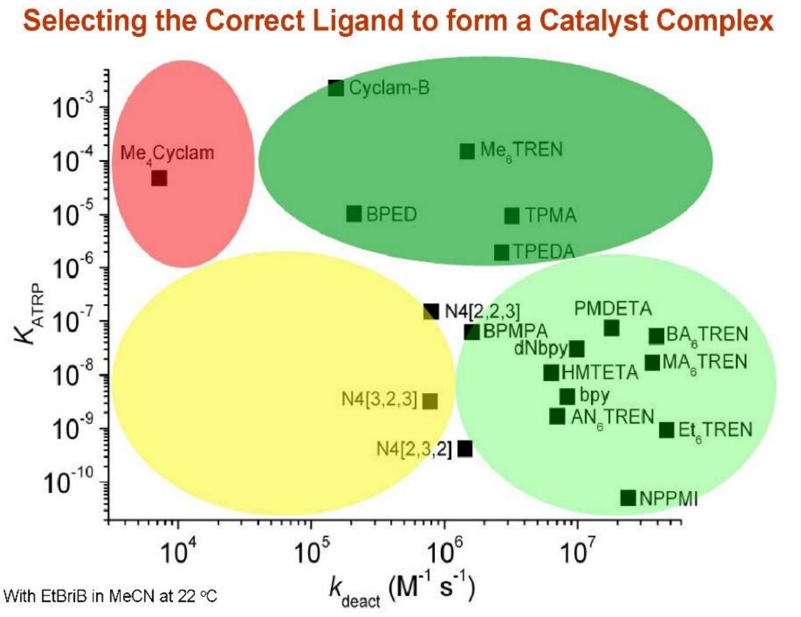

Figure 2.1 Rate of activation and deactivation for different ligands[35]

The most frequently used ligands are Me_6TREN and TPMA due to the fact that the catalyst complexes formed with these two ligands show large rate of deactivation and higher than that of activation.[25,35]

2.2.2.5 Kinetics of ATRP

The kinetics in ATRP can be deduced by presuming that the initiation is rapid and quantifiable and the termination processes can be neglect, as a result, the concentration of radicals will remain stable. The rate of polymerization, R_p, is proportional to the apparent rate constant, k_p^{app}, and the concentration of the monomer $[M]$, and thus is first order of concentration of monomer $[M]$, activator $[Cu(I)X]$, and initiator $[I]$ respectively, but is negatively first order with respect to the deactivator concentration $[Cu(II)X_2]$ (Eq 2.2).

$$R_p = k_p^{app}[M] = k_p K_{eq} \frac{[I][M][Cu(I)X]}{[Cu(II)X_2]} \qquad (Eq\ 2.2)$$

$$K_{eq} = \frac{k_{act}}{k_{deact}} = \frac{[R\cdot][Cu(II)X_2]}{[RX][Cu(I)X]} \qquad (Eq\ 2.3)$$

Increased initiator concentration results in a greater amount of propagating radicals and a decrease in degree of polymerization, which accelerates polymerization. The rate of polymerization also influenced by the ratio of $[Cu(I)X]/[Cu(II)X_2]$.

2.2.2.6 Shortcoming of ATRP

While ATRP has a number of advantages over traditional radical polymerization, it also have some disadvantages. The demand for a relatively large amount of the transition metal catalyst, which is then purified, complicates and raises the expense of industrial production. Additionally, leftover copper residues may color the product and may cause severe issues in certain applications, such as biological systems, due to copper's toxicity. Another problem is the reaction's extreme sensitivity to oxygen, which must be eliminated completely during degassing, further complicating and raising the cost of the reaction.[25,27,30]

2.3 Activator Regeneration Atom Transfer Radical Polymerization

Due to the high concentration of Cu catalyst used in the aforementioned ATRP procedures, issues of catalyst solubility, toxicity, and removal arose. At the same time, approaches have been employed to perform ATRP at reduced Cu concentrations without compromising kinetics or level of control. Because the rate of polymerization is proportional to the ratio of $[Cu(I)X]/[Cu(II)X_2]$ according to Eq 2.4, a lower copper concentration does not always imply a slower polymerization rate. However, the unavoidable termination reaction results in the accumulation of Cu(II), which causes the polymerization to slow down or stop. Thus, regeneration of Cu(I) is essential to maintain a healthy Cu(I)/Cu(II) ratio. These activator regeneration technologies enabled the use of lower copper concentrations and ligands at a cheaper cost. Additionally, the use of oxidatively stable Cu(II)Br_2 and oxygen tolerance sped up the reaction setup process significantly. The fundamental notion underlying activator regeneration is summarized in Scheme 2.4.[36]

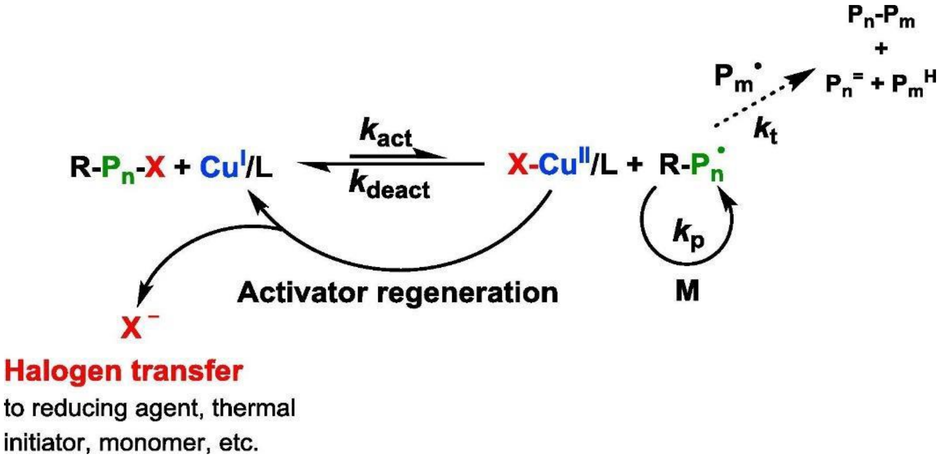

Scheme 2.4 Mechanism for activator regeneration ATRP.[36]

2.3.1 Activators regenerated by electron transfer (ARGET) ATRP

Activators regenerated by electron transfer (ARGET) ATRP makes use of chemical reducers such as ascorbic acid (AsAc) or Sn(II)R_2 compounds. The rate of polymerization is proportional to the concentration or rate of feeding of the reducing agent. Due to its durability and excellent oxygen tolerance, ARGET ATRP was widely employed in the synthesis of polymer-inorganic hybrid materials.

2.3.2 Initiators for continuous activator regeneration (ICAR) ATRP

Initiators for continuous activator regeneration (ICAR) ATRP employs a thermal radical initiator such as AIBN, whose slow disintegration constantly converts the deactivator back to the activator.[37] The dynamics of an ICAR ATRP are identical to those of RAFT, with the exception that a small proportion of the chains come from the thermal initiator. As a result, it is not optimal for synthesizing well-defined block copolymers.

2.3.3 Electrochemically mediated ATRP (*e*ATRP)

Electrochemically mediated ATRP (eATRP) makes use of electrochemical current. eATRP requires no external chemicals, making it a "cleaner" technique than ARGET or ICAR.[31,38] eATRP's downsides include its complicated reaction setup, high cost of supporting electrolytes, and difficulties scaling up.

2.3.4 Supplemental activator and reducing agent (SARA) ATRP

Supplemental activator and reducing agent (SARA) ATRP employs zero-valent copper as a supplementary activator as well as a reducing agent.[31,39] Polymerization proceeds at a rate determined by the surface area of Cu(0). Cu metal is recyclable and may be used in a variety of reactions.

2.3.5 Photo ATRP

UV or visible light lowers excited Cu(II) complexes to a free aliphatic amine, which is typically an excess of ligand in photo ATRP.[40] The ratio of ligand to copper has an effect on the rate of polymerization. As with eATRP, photo ATRP accomplished temporal control through the use of light as an external stimulus.[41] Recently, several organ catalysts, such as 10-phenylphenothiazine (PTZ), have been shown to be effective photocatalysts for photo ATRP.[42,43]

Chapter III Synthesis of linear-*hybrid* bottlebrush-linear (LhBBL) triblock copolymers

3.1 Synthesis of linear-*hybrid* bottlebrush-linear (LhBBL) triblock copolymers

In this study, I seek to independently control the stiffness and extensibility of elastomers by employing the self-assembly of architecturally designed bottlebrush-based ABA triblock copolymers which I named it as linear-*hybrid* bottlebrush-linear (LhBBL) triblock copolymers. To achieve this synthesis, I choose polymerize monomethacryloxypropyl terminated polydimethylsiloxane (mMAPDMS) as low T_g side-chains and poly (benzyl methacrylate) (PBnMA) as high T_g end blocks and spacers to synthesize a linear-hybrid bottlebrush-linear triblock copolymer as shown in Figure 3.1.

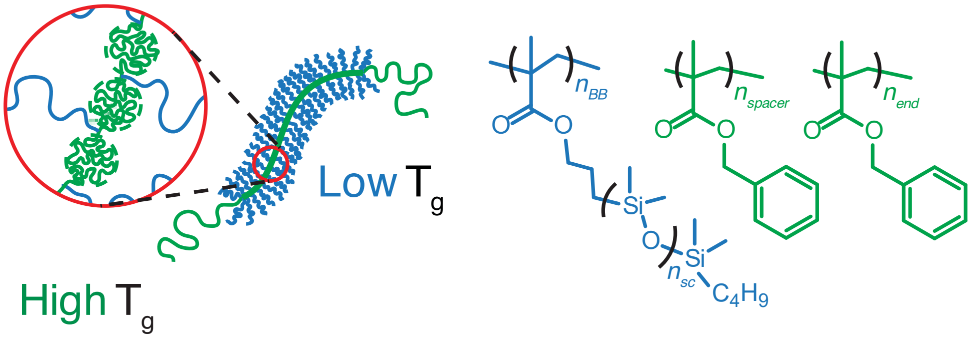

Figure 3.1 Linear-*hybrid* bottlebrush-linear (LhBBL) triblock copolymers and chosen of monomers.

In which n_{BB} is the number of side-chain per middle block, n_{spacer} is the number of BzMA spacers per middle block and n_{end} is the number of BzMA on each end block. There are two reasons for us to choose PDMS and PBzMA. First, PDMS has a low T_g, about -125 ^oC, whereas PBzMA has a T_g, about 60 ^oC, the large difference between T_g of PDMS and PBzMA assures the thermal stability of the self-assembled elastomer over a wide range of temperature. Besides this, PDMS and PBzMA are highly incompatible with a large Flory-Huggins interaction parameter of 0.54 such that microphase separation of the triblock copolymer easily falls into the strong segregation limit. In comparison to the weak segregation constraint, within the strong segregation limit the microstructure is much more stable and less sensitive to processing fluctuations, enabling controllable macroscopic properties.

Typical ATRP is oxygen-sensitive and requires a high concentration of metal catalyst to preserve the activity throughout the polymerization reaction, resulting in an unavoidable metal residue in the final products that is toxic to physiological systems, furthermore, traditional ATRP is hard to precisely control the synthesis of bottlebrush polymer with large molecular weight. To obtain expected, well-designed, reasonable and clean product, I choose a newly designed Activators regenerated by electron transfer (ARGET) atom transfer radical polymerization (ATRP) method in which the catalysts are continuously regenerated with the existence of reducing reagents. This increases oxygen tolerance and greatly reduces the catalyst concentration necessary for the copolymerization of brush PDMS monomers and BnMA monomers.

3.1.1 Synthetic route of linear-*hybrid* bottlebrush-linear (LhBBL) triblock copolymers

Contrary to conventional synthesis approaches that begin with monomers, I employ a macromonomer-based approach to create the copolymer. The synthetic route of linear-*hybrid* bottlebrush-linear (LhBBL) triblock copolymers includes two steps as illustrated in Scheme 3.1: in step I, I first synthesize the middle *hybrid* bottlebrush block copolymer through copolymerization of polymerize monomethacryloxypropyl terminated polydimethylsiloxane (mMAPDMS) and benzyl methacrylate (BnMA) with a bifunctional initiator; in step II, I use middle *hybrid* bottlebrush block copolymer synthesized in step I as a macro-initiator to further grow the end linear blocks on two ends of it. After completing both procedures, a PBnMA$_y$-*b*-(BnMA$_x$-*r*-PDMS)$_m$-*b*-BnMA$_y$ triblock copolymer is formed.

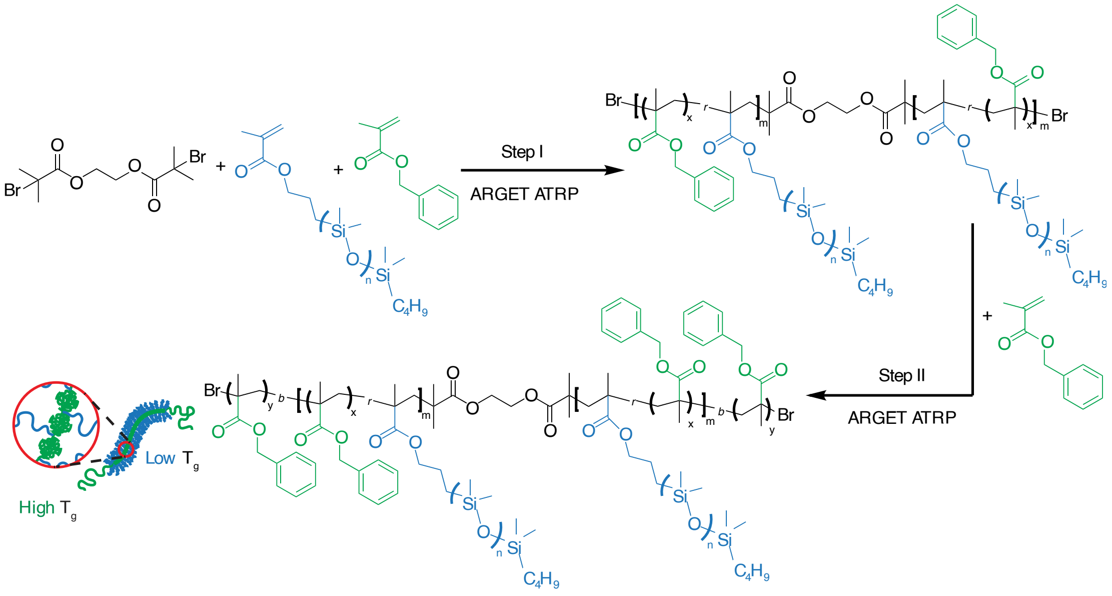

Scheme 3.1 Synthetic route of linear-*hybrid* bottlebrush-linear (LhBBL) triblock copolymer: Step I, synthesis of middle *hybrid* bottlebrush (*h*BB)block copolymer; Step II: Synthesis of linear-*hybrid* bottlebrush-linear (LhBBL) triblock copolymer

3.1.2 Designed parameters of linear-*hybrid* bottlebrush-linear (LhBBL) triblock copolymers

In Chapter I I hypothesize that linear-*hybrid* bottlebrush-linear (LhBBL) triblock copolymers will self-assemble to a network structure in which the stiffness of the network is controlled by the number of brush monomers while the extensibility of the network depends on the total number of space monomers and brush monomers. To testify this hypothesis, I only need to vary the number of spacer monomers while keeping all the others constant. Hence, I choose polymerize monomethacryloxypropyl terminated polydimethylsiloxane (mMAPDMS) with average molar mass of 1000 g/mol (MCR-M11) and keep the number brush monomers 200 per chain. To ensure the copolymer self-assemble into a network structure, I targeted the weight fraction of end blocks to side-chains around 6% which will result in triblock copolymer with 36 BnMA unit on each end chain as shown in Table 3.1. The only variation will be the ratio between space monomers and side-chain monomers, x :

$$x = \frac{n_{spacer}}{n_{BB}} \qquad (Eq\ 3.1)$$

Sample	$x=n_{spacer}/n_{BB}$	n_{BB}	n_{spacer}	n_{end}	$f_{BnMA}=M_{two\ end}/MW_{BB}$
1	0	200	0	36	0.06
2	0.3	200	60	36	0.06
3	0.6	200	120	36	0.06
4	0.9	200	180	36	0.06
5	1	200	200	36	0.06
6	1.2	200	240	36	0.06
7	1.5	200	300	36	0.06
8	2	200	400	36	0.06

Table 3.1 Designed parameter of linear-*hybrid* bottlebrush-linear (LhBBL) triblock copolymers

3.1.3 Chemicals and materials

MCR-M11, average molar mass 1000 g/mol, was bought from Gelest and purified through basic alumina columns to eliminate inhibitors. Copper(II) chloride ($CuCl_2$, 99.999%), Copper(II) bromide ($CuBr_2$, 99.999%), Benzyl methacrylate

(BnMA, 96%), *tris*[2-(dimethylamino)ethyl]amine (Me_6TREN), Tin(II) 2-ethylhexanoate ($Sn(EH)_2$, 92.5 – 100%), ethylene bis(2-bromoisobutyrate) (2-BiB, 97%), xylene (≥99.7%), anisole (≥99.7%) and dimethylformamide (DMF) were bought from Sigma Aldrich and used as arrived. Methanol (Certified ACS), Toluene (Certified ACS), tetrahydrofuran (THF, Certified ACS) and THF (HPLC grade), were bought from Fisher and used as arrived.

3.1.4 Synthetic procedures.

Here, I use sample, $BnMA_{40}$-*b*-($BnMA_{0.31}$-*r*-$PDMS^1$)$_{195}$-*b*-$BnMA_{40}$, as an example to describe the detail of synthesis protocol. The synthesis of other samples are described in supporting information.

Step I. Synthesis of hybrid bottlebrush block copolymer.

A 50 mL Schlenk flask is charged with difunctional initiator (2-BiB, 5.76 mg, 0.016 mmol), macromonomer (MCR-M11, 8 g, 8 mmol), space monomer (BnMA, 0.577 g, 3.278mmol), xylene (14 mL) and anisole (14 mL). To increase the solubility of catalyst in reaction, a catalyst solution is prepared in advance by dissolving ligand (Me_6TREN, 46 mg, 0.2 mmol) and catalyst ($CuBr_2$, 4.5 mg, 0.02 mmol) in 1 mL DMF. Then, 160 µL catalyst solution, containing 0.032 mmol Me_6TREN and 0.0032 mmol $CuBr_2$, is added to the mixture. The mixture is bubbled with nitrogen for 60 mins to remove oxygen. Afterwards, reducing agent (Sn $(EH)_2$, 51.8 mg, 0.128 mmol) in 100 µL xylene is quickly dropped into the Schlenk flask through a syringe. The flask is sealed when the nitrogen is still bubbling, and then immersed in an oil bath at 60 °C. I take a small amount of mixture to determine the conversion of side-chain monomer per hour to monitor the reaction and calculate the termination time for targeted product.

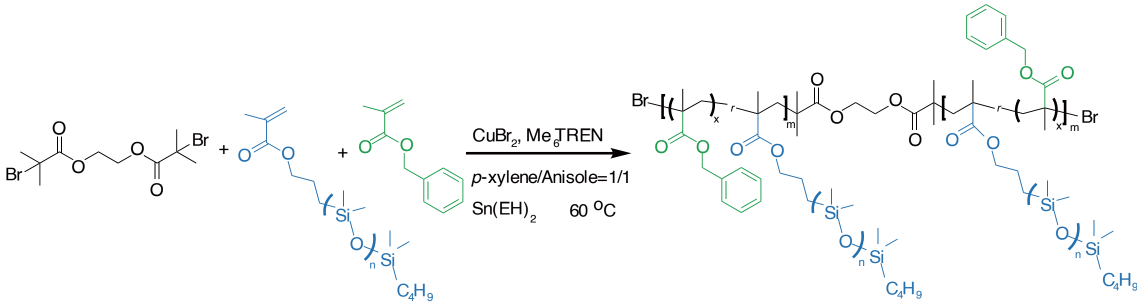

Scheme 3.2 Synthesis of *hybrid* bottlebrush (hBB) copolymer

Once the conversion reach the expected point, the reaction is stopped by opening to air and cooling down to room temperature. To remove the catalyst, the remaining reaction mixture is passed through a neutral alumina column with THF. A rotary evaporator (Buchi R-205) is used to concentrate the collected solution. To remove the unreacted monomers from the *hybrid* bottlebrush copolymer, the mixture was precipitated in Methanol for 5 times to assure that all monomers and impurities are completely removed. After the purification, I use proton nuclear magnetic resonance (^{1}H NMR) spectra to measure the number of spacers and use gel permeation chromatography (GPC) to measure the polydispersity index (PDI) of the final product. At room temperature, the product is a transparent, viscous liquid.

Step II. Synthesis of LhBBL triblock copolymers.

A 50 mL Schlenk flask is charged with macroinitiator (0.729 g, 0.0035 mmol) synthesized in step I, monomer (BnMA, 437 mg, 2.48 mmol), xylene (4.2 mL) and anisole (2.1 mL). Me$_6$TREN (46 mg, 0.2 mmol) and CuBr$_2$ (4.5 mg, 0.02 mmol) are dissolved in 1 mL DMF to make a catalyst solution. Then, 53 µL catalyst solution, which contains 0.01 mmol Me$_6$TREN and 0.001 mmol CuBr$_2$, is added to the mixture. The solution is bubbled with nitrogen for one hour to remove oxygen. Afterwards, reducing agent (Sn(EH)$_2$ 8.1 mg, 0.02 mmol) with 100 µL xylene is quickly dropped to the reaction mixture when the nitrogen is still bubbling. Then, the flask is sealed and immersed in an oil bath at 60 °C. The reaction is monitored using NMR per hour to calculate the conversion of BnMA and determine the stop time.

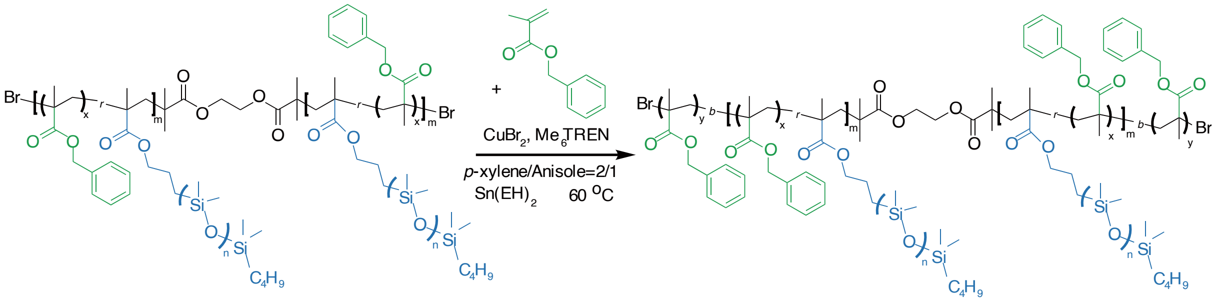

Scheme 3.3 Synthesis of linear-*hybrid* bottlebrush-linear (LhBBL) triblock copolymer

After the reaction, the reaction mixture is passed through a neutral aluminum oxide column with THF to remove the residual catalyst, and a rotary evaporator is used to concentrate the collected solution. The polymer is precipitated in methanol for another five times to remove the unreacted monomers. After purification, the sample is dried in a vacuum oven at room temperature for 12 hours. The dried polymer is used for ^{1}H NMR analysis to calculate the number of BnMA per end chain and GPC analysis. The LhBBL triblock copolymer is a transparent, elastic solid.

3.2 Characterization and discussion

3.2.1 Characterization instruments

3.2.1.1 Proton nuclear magnetic resonance spectroscopy (^{1}H NMR).

I use ^{1}H NMR to determine the number of side chains per bottlebrush n_{BB}, number of spacers per bottlebrush n_{spacer}, and the number BnMA per end chain n_{end}. NMR characterization is performed using Shamu-500 MHz spectrometer. All the samples are characterized in $CDCl_3$. Chemical shifts for ^{1}H NMR spectra are relative to a singlet at 7.26 ppm in $CDCl_3$.

3.2.1.2 Gel permeation chromatography (GPC).

I use GPC to determine the PDI of polymers. GPC measurements are performed using TOSOH EcoSEC HLC-8320GPC system with two TOSOH Bioscience TSKgel GMH_{HR}-M 5μm columns in series and a refractive index detector at 40°C. HPLC grade tetrahydrofuran is used as the eluent with a flow rate of 1mL/min. The calibration curve is obtained using standard polystyrene (PS) samples. The samples are dissolved in THF with a concentration of 3mg/mL.

3.2.1.3 Small-angle scattering (SAXS)

SAXS measurements are carried out using synchrotron source at 12-ID beamline of Brookhaven National Laboratory. To prepare thin films with controlled, uniform thicknesses, I dissolve the sample in Toluene with a concentration of 1 g/ml and purify the polymer solution by passing through a syringe filter with membrane pore size 0.45 μm. Then I drop 100 **μ**l solution onto a glass substrate with dimension of 10 x 10 x 1 mm (length x width x thickness). After the solvent been evaporated for overnight, the bulk sample with thickness around 1 mm will be ready on the glass slide.

3.2.2 Results and discussion

3.2.2.1 Molecular parameters of LhBBL copolymers

We use ^{1}H NMR to determine the molecular parameter of the LhBBL copolymers including number of side chains per bottlebrush n_{BB}, number of spacers per bottlebrush n_{spacer}, spacer/side-chains ratio x and the number of BnMA per end chain n_{end}. Here, I will use the sample $BnMA_{40}$-*b*-($BnMA_{0.31}$-*r*-$PDMS^1$)$_{195}$-*b*-$BnMA_{40}$ as an example to describe the detail calculations.

To calculate the number of side chains per bottlebrush n_{BB}, I utilize the ^{1}H NMR spectrum of raw mixture of ARGET ATRP of poly($BnMA_{0.31}$-*r*-PDMS)$_{195}$ as shown in Figure 3.2. The peak around 4.2 ppm represents the protons on carbon connected with the methyl methacrylate group showing as a. It should be noted that only the macromonomers will have such a peak, when the macromonomer been polymerized, the peak will shift downwards. However the peak around 0.7 ppm represents the protons on two carbons connected with two silicon atoms in both monomer and polymer (as shown in b) since the protons on these two carbon atoms are far away from the methyl methacrylate group, the chemical shift of them will not be influenced by the breakage of double bond. Hence, I can use the integration of peak a and b to calculate the conversion rate of brush monomers.

$$conversion\ rate\ of\ PDMS = (1 - Area(a) \times 2/Area(b)) \times 100\% \qquad (Eq\ 3.2)$$

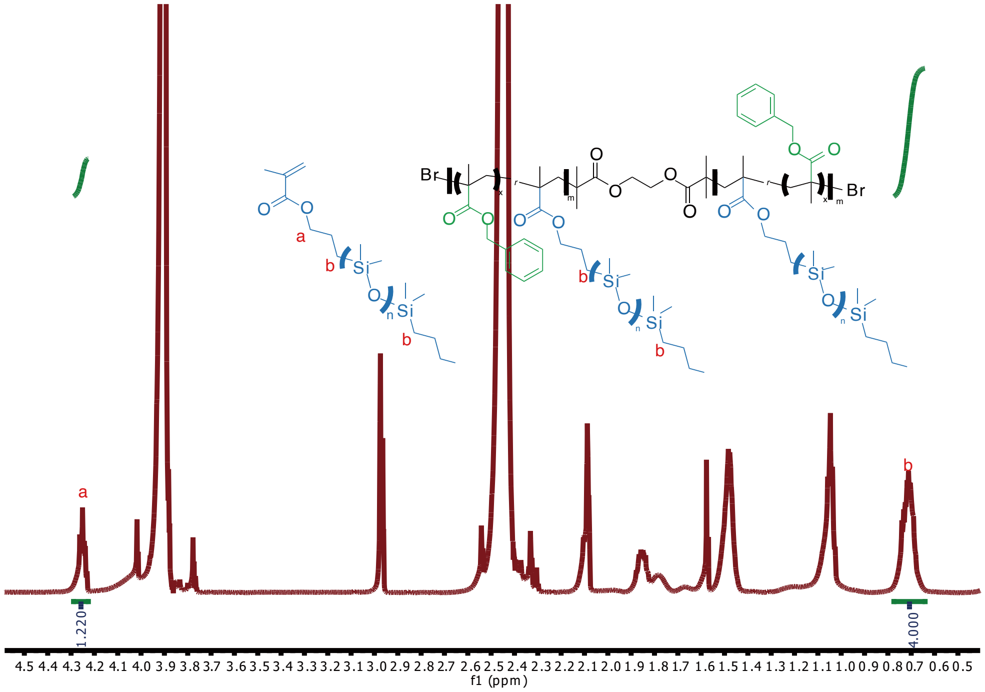

Figure 3.2. ^{1}H NMR spectrum of raw mixture of ARGET ATRP of poly(BnMA$_{0.31}$-*r*-PDMS)$_{195}$ (CDCl$_3$, 25°C). $Conversion\ rate\ of\ PDMS\ side\ chain = (1 - Area(a) \times 2/Area(b)) \times 100\% = 39\%$. DP of PDMS side chain is 195.

During the experiment, I found that the reaction only follows the rule of ARGET ATRP at a moderate conversion rate of macromonomers since the solubility of the copolymer will decrease with the increasing of molecular weight. As a result, for each reaction of middle block, I target at a conversion rate of 40% which requires an initial feeding ratio between PDMS to initiator of 500:1 so that the final DP of side-chains will be 200 at a conversion rate of 40%. The degree of polymerization (DP) of side-chains can be calculated from the conversion rate as following:

$$n_{BB} = 500 \times conversion\ rate\ of\ PDMS \qquad (Eq\ 3.3)$$

To calculate the number of spacers per bottlebrush n_{spacer}, I utilize the ^{1}H NMR spectrum of purified poly(BnMA$_{0.31}$-*r*-PDMS)$_{195}$ as shown in Figure 3.3. The peak around 5.0 ppm represents the protons on carbon connected with the benzyl group of spacers showing as a. While the peak around 0.7 ppm represents the protons on two carbons connected with two silicon atoms as shown in b. Hence, I can use the integration of peak a and b to calculate the DP of spacers.

$$n_{spacer} = n_{BB} \times Area(a) \times 2/Area(b) \qquad (Eq\ 3.4)$$

Thus I can obtain the spacer/side-chain ratio:

$$x = \frac{n_{spacer}}{n_{BB}} \qquad (Eq\ 3.5)$$

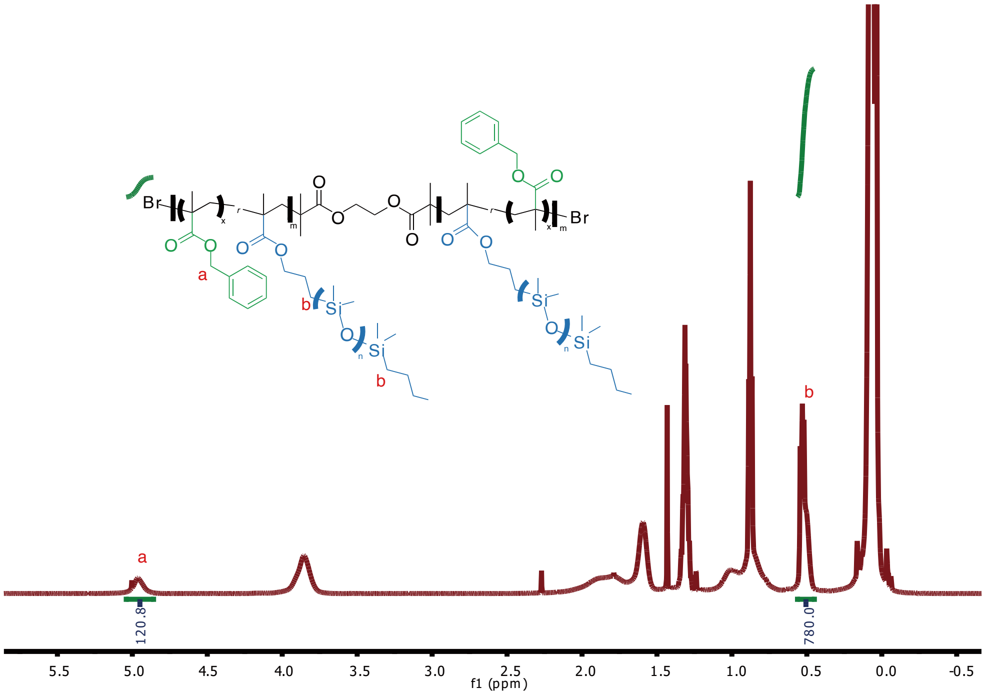

Figure 3.3 ^{1}H NMR spectrum of poly(BnMA$_{0.31}$-*r*-PDMS)$_{195}$ (CDCl$_3$, 25°C). $DP\ of\ spacers = DP\ of\ middle\ block \times Area(a) \times 2/Area(b) = 60$. Spacer/side chain ratio, x, is 0.31.

To calculate the number of BnMA per end chain n_{end}, I utilize the ^{1}H NMR spectrum of purified BnMA$_{40}$-*b*-(BnMA$_{0.31}$-*r*-PDMS)$_{195}$-*b*-BnMA$_{40}$ as shown in Figure 3.4. The peak around 5.0 ppm represents the protons on carbon connected with the benzyl group of both spacers and end chains showing as a. While the peak around

0.7 ppm represents the protons on two carbons connected with two silicon atoms as shown in b. Hence, I can use the integration of peak a and b to calculate the number of BnMA per end chain n_{end}.

$$n_{end} = (n_{BB} \times 2 \times \frac{Area(a)}{Area(b)} - n_{spacer})/2 \qquad (Eq\ 3.5)$$

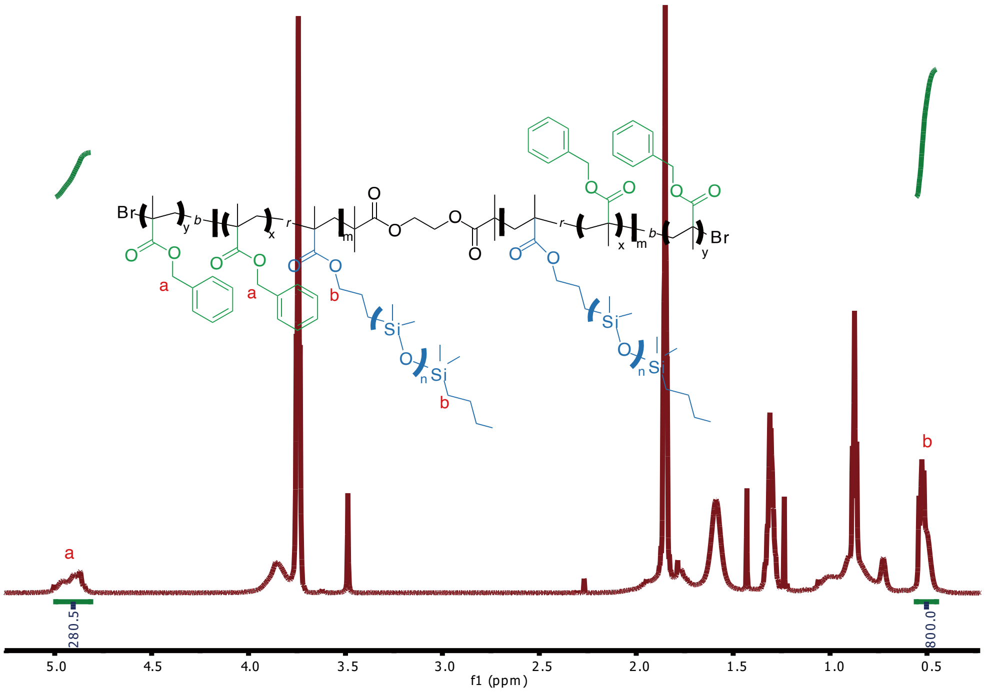

Figure 3.4 ^{1}H NMR spectrum of BnMA$_{40}$-*b*-(BnMA$_{0.31}$-*r*-PDMS)$_{195}$-*b*-BnMA$_{40}$ (CDCl$_3$, 25°C). $DP\ of\ each\ BnMA\ end\ block = (DP\ of\ sidechain \times 2 \times \frac{Area(a)}{Area(b)} - DP\ of\ spacer)/2 = 40$. Weight fraction of end chains to side-chains is around 6.7%.

With those parameters, I can calculate the weight fraction of end chains compared with side-chains:

$$wt_{end}\% = \frac{2 * n_{end} * 176\frac{g}{mol}}{n_{BB} * 1000\frac{g}{mol}} * 100\% \qquad (Eq\ 3.6)$$

After synthesis, 10 samples are obtained, the parameters of all the sample are listed in Table 3.2.

Sample	Middle block		Triblock	
	n_{sc}	n_{spacer}/n_{BB}	n_{BzMA}(each end)	$f_{BnMA}(MW_{end}/MW_{sc})$
$BnMA_{36}$-*b*-$PDMS_{205}$-*b*-$BnMA_{36}$	205	0.00	36	5.8%
$BnMA_{40}$-*b*-($BnMA_{0.31}$-*r*-PDMS)$_{195}$-*b*-$BnMA_{40}$	195	0.31	40	6.7%
$BnMA_{33}$-*b*-($BnMA_{0.6}$-PDMS)$_{200}$-*b*-$BnMA_{33}$	200	0.60	33	5.5%
$BnMA_{42}$-*b*-($BnMA_{0.83}$-*r*-PDMS)$_{200}$-*b*-$BnMA_{42}$	200	0.83	42	6.9%
$BnMA_{34}$-*b*-($BnMA_{0.88}$-*r*-PDMS)$_{200}$-*b*-$BnMA_{34}$	200	0.88	34	5.6%
$BnMA_{33}$-*b*-($BnMA_{1}$-*r*-PDMS)$_{200}$-*b*-$BnMA_{33}$	200	1.00	33	5.5%
$BnMA_{30}$-*b*-($BnMA_{1.26}$-*r*-PDMS)$_{190}$-*b*-$BnMA_{30}$	190	1.26	30	5.3%
$BnMA_{31}$-*b*-($BnMA_{1.42}$-PDMS)$_{190}$-*b*-$BnMA_{31}$	190	1.42	31	5.4%
$BnMA_{20}$-*b*-($BnMA_{1.48}$-*r*-PDMS)$_{200}$-*b*-$BnMA_{20}$	200	1.48	20	3.4%
$BnMA_{23}$-*b*-($BnMA_{2.15}$-*r*-PDMS)$_{200}$-*b*-$BnMA_{23}$	200	2.15	23	3.9%

Table 3.2 Chemical parameters of LhBBL copolymers

3.2.2.2 Kinetics of the reactions

We use ^{1}H NMR to monitor two-step reactions and study the relationship between conversion rate of monomer and reaction time, thus I can estimate the time to stop the reaction for obtaining the expected product. Here, I will use the sample ($BnMA_{0.31}$-*r*-$PDMS^{1}$)$_{195}$ as an example to describe the detail calculations.

Since ARGET ATRP follows the rule of first order reaction, the relationship between monomer concentration and reaction time can be calculated as following

$$Rate = \frac{d[M]}{dt} = -k[M] \qquad (Eq\ 3.7)$$

$$\int \frac{d[M]}{[M]} = -k \int dt \qquad (Eq\ 3.8)$$

$$ln \frac{[M]}{[M]_0} = -kt \qquad (Eq\ 3.9)$$

$$t = \frac{1}{k} ln \frac{[M]_0}{[M]} \qquad (Eq\ 3.10)$$

In which $[M]$ is the current concentration of monomer, $[M]_0$ is initial concentration of monomer, k is rate constant, t is reaction time.

In section **3.5.2.1**, I discussed how to use NMR calculated the conversion rate of PDMS during reaction. The reaction is monitored at different time spot and $ln \frac{[M]_0}{[M]}$ is obtained as shown in Table 3.3.

Reaction time	Conversion rate (%)	ln([M]$_0$/[M])
63	5.7	0.05869
128	13.6	0.1456
185	24.0	0.2744
308	36.3	0.45099
346	40.8	0.52425

Table 3.3 Kinetics for polymerization of (BnMA$_{0.31}$-*r*-PDMS^1)$_{195}$

Figure 3.5 plots the relationship between reaction time, t, and $ln \frac{[M]_0}{[M]}$. The linear relationship indicates that the reaction is first order reaction and the reaction can be monitored to find expected stop time.

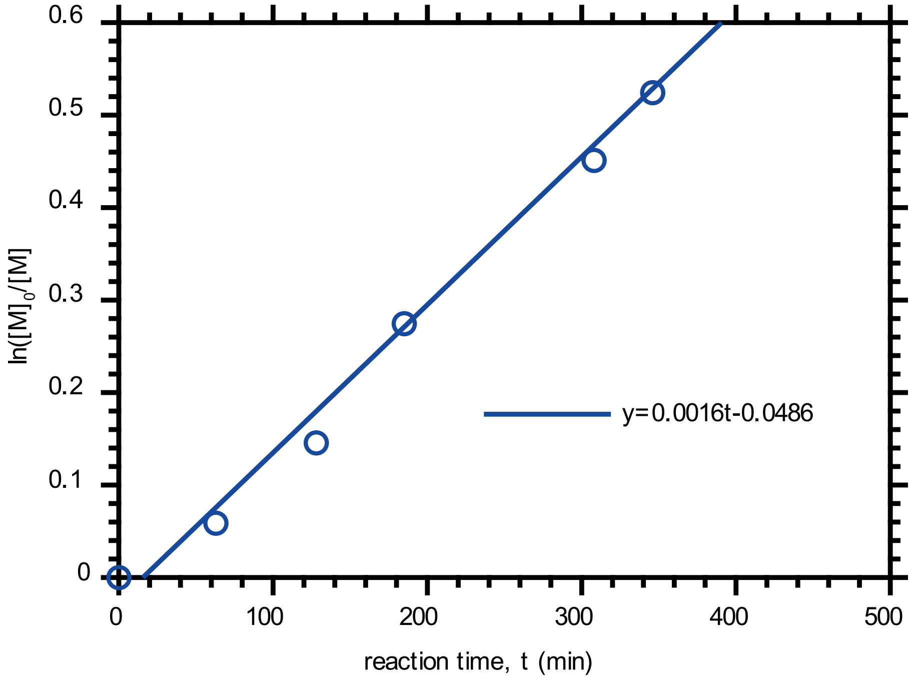

Figure 3.5 Kinetics for polymerization of $(BnMA_{0.31}\text{-}r\text{-}PDMS^{1})_{195}$

Then the kinetics of all the middle hybrid bottlebrush copolymers are plotted in Figure 3.6. The linear relationship between reaction time, t, and $ln\frac{[M]_0}{[M]}$ indicates that all the reactions are followed the rule of first order reaction. Furthermore, the similar slopes of all the samples indicates that the rate of propagation of macromonomers within the copolymerize of macromonomers and small monomers mainly depends on the concentration of macromonomers and independent of the concentration of small monomers.

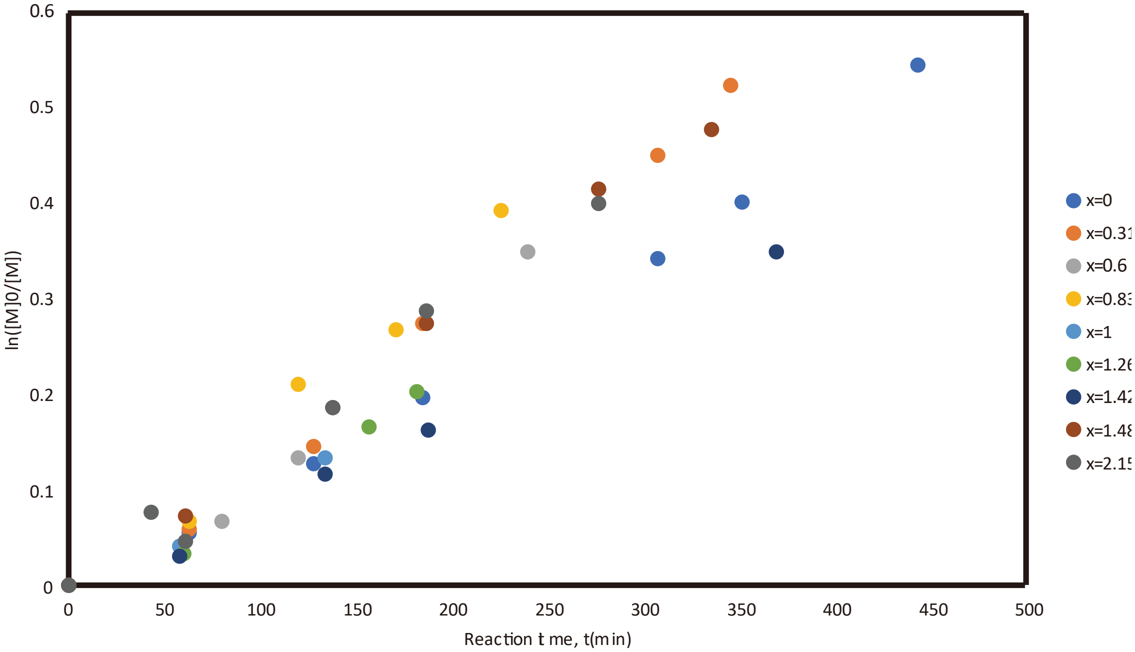

Figure 3.6 Kinetics for hybrid bottlebrush copolymers

3.2.2.3 Study of spacer/side-chain ratios

To get a better control on the reactions, I extract the relationship between initial feeding ratio (molar ratio between spacer monomers and bottlebrush monomers) and final spacer/side-chain ratio, x as shown in Table 3.4. Figure 3.7 plots the above relationship. Final spacer/side-chain ratio, x, is linear proportional to the initial feeding ratio, which provide a guidance for the further study of synthesizing samples with different spacer/side-chain ratio.

Initial $[M_{spacer}]/[M_{BB}]$	$x=n_{spacer}/n_{BB}$
0	0.00
0.21	0.31
0.41	0.60
0.52	0.83
0.54	0.88
0.66	1.00
0.8	1.26
0.9	1.42
1	1.48
1.4	2.15

Table 3.4 Relationship between final spacer/side-chain ratio and initial feeding ratio

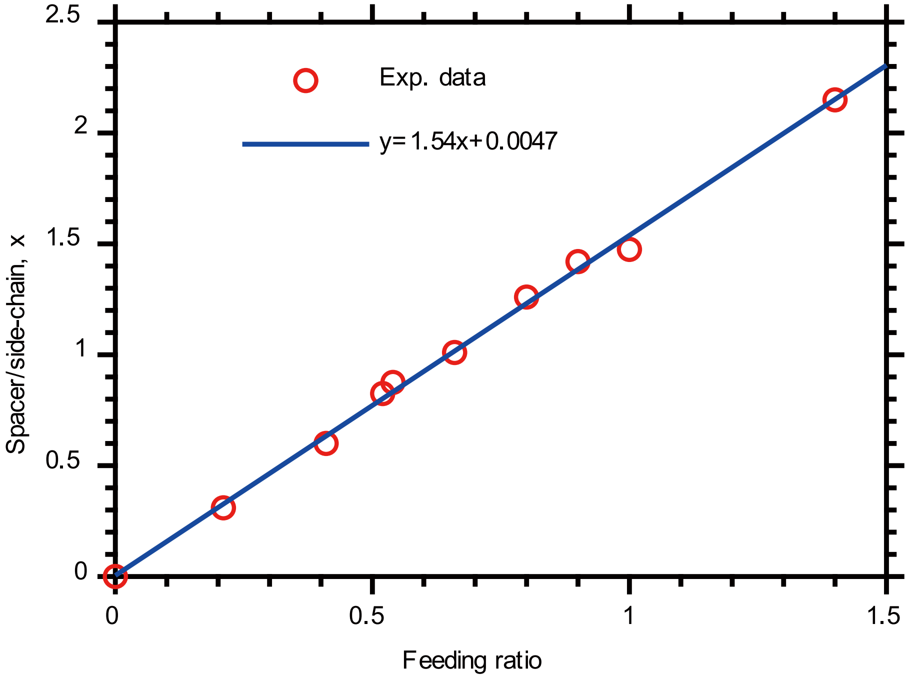

Figure 3.7 Relationship between final spacer/side-chain ratio and initial feeding ratio

3.2.2.4 Microstructure of LhBBL copolymer

The scattered plots of SAXS measurement of LhBBL copolymer samples are shown in Figure 3.8. The position of first peak is around 0.17 nm^{-1} gives a length scale of 36.9 nm ($d = 2\pi/q$). The pronounced scattering peaks suggest a random sphere network structure. However, these needs to be further proved using transmission electron microscopes (TEM) or atomic force microscopy (AFM).

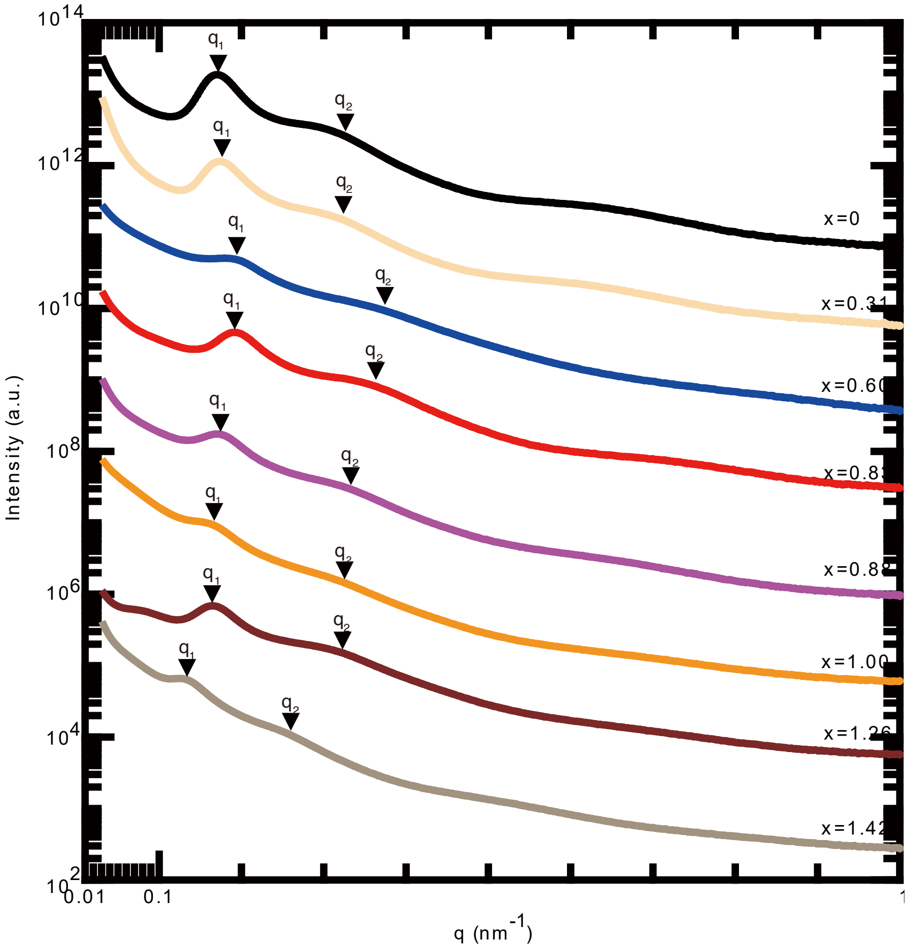

Figure 3.8 SAXS measurements of LhBBL copolymers

3.3 Mechanical behavior measurement

3.3.1 Tensile test

Tensile test are performed using MARK-10 ESM303 Motorized Tension/Compression Test Stand with a MARK-10 M5-05 force gauge. The samples are dissolved in THF with a concentration around 1 mg/mL. The solution is continuously poured into a rectangular shape Teflon mold to avoid bubbles. After the solvent been evaporated, the bulk polymer is pealed from the mold and put onto a glass substrate. Then I use a compression machine and a dog-bone shape die (as shown in Figure 3.9) to cut the bulk polymer to get a standard dog-bone shape sample for tensile test. Since the polymers are too soft to be grab by the clamps directly, I use epoxy to glue two ends of the dog-bone shape sample with cardboard and use clamps to grab the cardboard to avoid destroying the polymers. The tensile test is performed at room temperature with a constant speed, 14.4 mm/min (Strain rate: 2%/s).

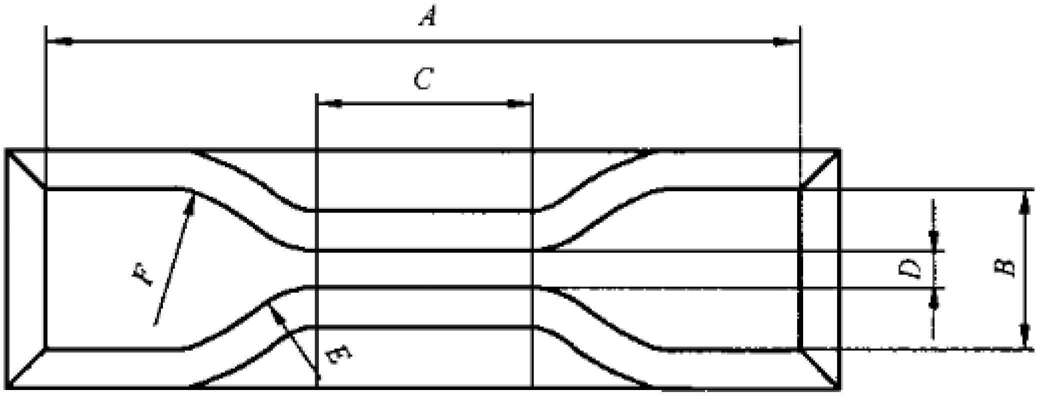

Figure 3.9 Schematic diagram of dog-bone shape die with dimension of: Total length A = 35 mm; End width B = 6.0±0.5 mm; Bridge length C = 12.0±0.5 mm; Bridge width D = 2.0±0.1 mm;

Radius of outside transition edge E = 3.0±0.1 mm; Radius of inside transition edge F = 3.0±0.1 mm

3.3.2 Stress-strain behavior of LhBBL triblock copolymers

The video of tensile test measurement can be found in supplementary material. The stress-strain curve of LhBBL copolymer sample with spacer/side-chain ratio, x, ranging from 0 to 1.42 are plotted in Figure 3.10. All the samples show an interesting elastomeric properties which includes extreme softness with Young's modulus about several thousand Pa and large elongation at break ranging from 100%-1200%.

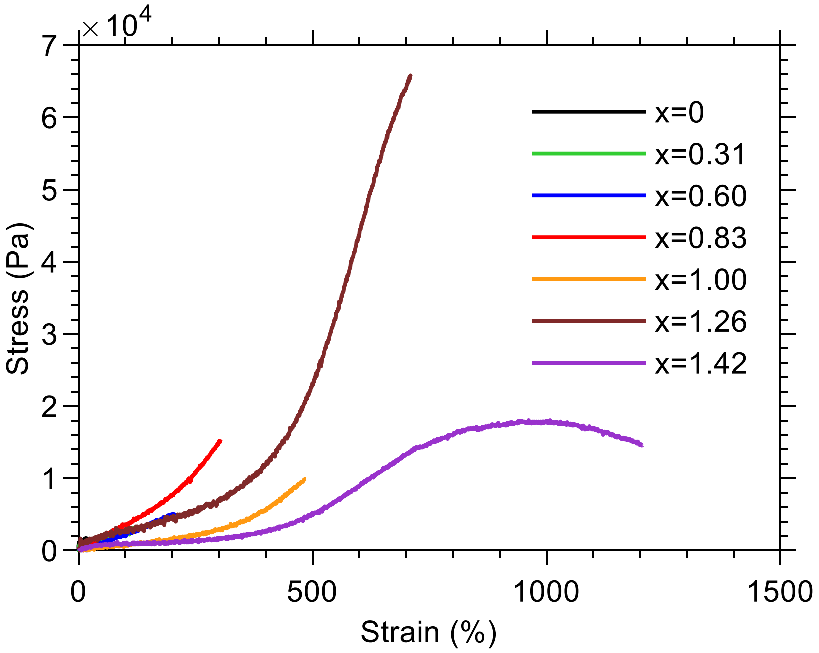

Figure 3.10 Stress strain curve of LhBBL copolymer sample with spacer/side-chain ratio, x, ranging from 0 to 1.42.

The Young's modulus can be extracted from the slope of initial elastic regime. As well as the elongation at break can be read from the plots. The mechanical behavior of LhBBL copolymers are listed in Table 3.5.

Spacer/side-chain, x	Young's modulus (Pa)	Elongation at break (%)
0.00	2723	20
0.31	2174	124
0.60	2420	206
0.83	4336	304
1.00	880	486
1.26	1951	710
1.42	1555	1205

Table 3.5 Mechanical behavior of LhBBL copolymer

To visualize the dependence of stiffness on spacer/side-chain ratio, I plotted Young's modulus versus spacer/side-chain ratio as shown in Figure 3.11. The Young's modulus of sample is independent on spacer/side-chain ratio, which proves that the stiffness remain constant with the existence of spacer domains.

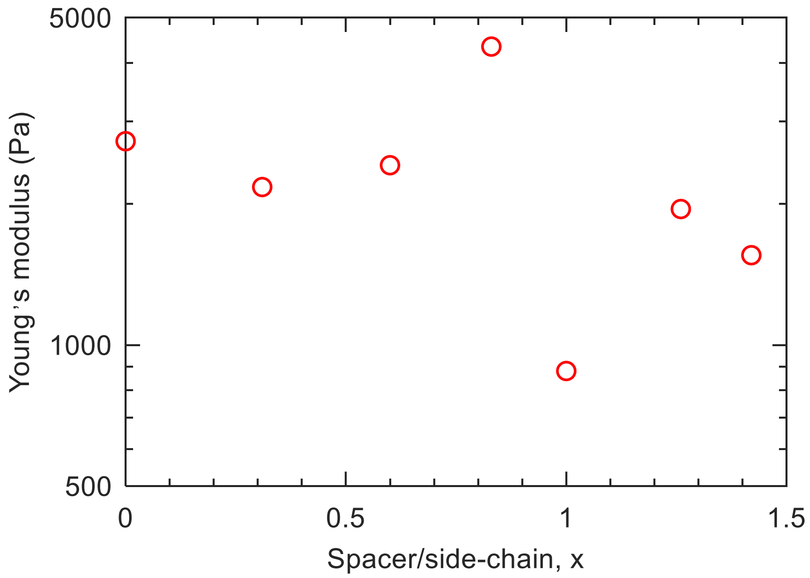

Figure 3.11 Plot of Young's modulus vs spacer/side-chain ratio

Figure 3.12 plots the relationship between extensibility and the spacer/side-chain ratio of LhBBL copolymers. Interestingly, the elongation at break increase exponentially with spacer/side-chain ratio. This illustrates the fact that the stiffness of the network remain constant while the extensibility increasing.

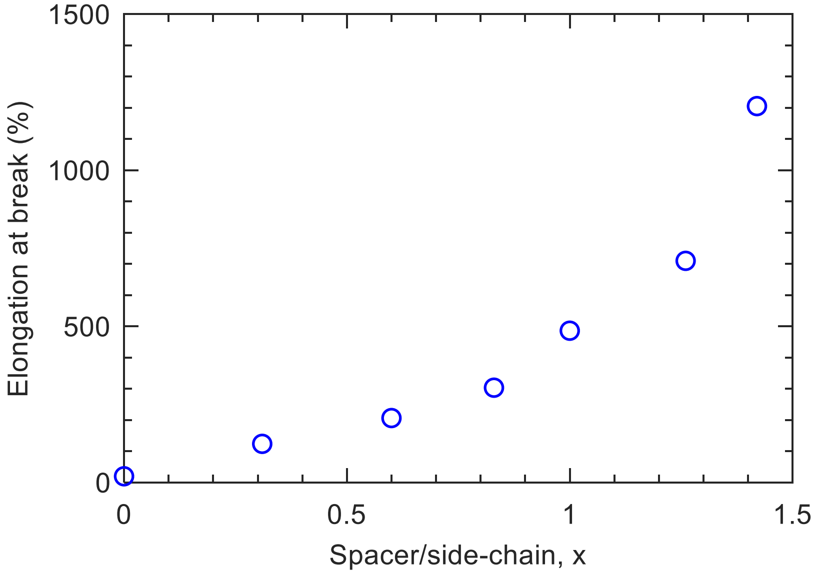

Figure 3.12 Plot of elongation at break vs spacer/side-chain ratio.

This unique stress-strain behavior that independently control stiffness and extensibility of polymer network breaks the traditional understanding which for a polymer network with smaller number of units per network strand, the stiffness is higher whereas the extensibility is smaller. The LhBBL copolymer in this study exhibits an ability to control the stiffness constant through keeping the number of side-chain constant, in the meanwhile, increase the extensibility by adding small spacers into network strands.

3.3.3 Additional study on mechanical behaviors.

From the Figure 3.10, toughness can be obtained by integration of the area below the stress-strain curve. Similar to extensibility, toughness of LhBBL copolymer increases exponentially with spacer/side-chain ratio as shown in Figure 3.13. The material become tougher with the adding of spacers.

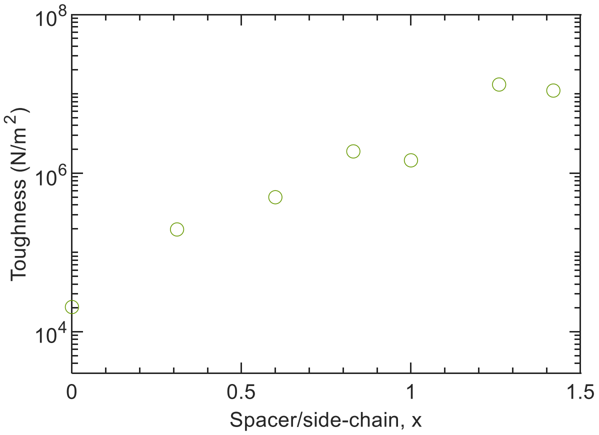

Figure 3.13 Plot of toughness vs spacer/side-chain ratio.

The phenomenon becomes more interesting when the spacer/side-chain ratio becomes higher than 2. Figure 3.14 is the stress-strain curve of sample with spacer/side-chain ratio of 2.15. The behavior illustrates it as a plastic polymer, which indicates that the independent control over stiffness and extensibility has a limit of the fraction of spacers. However, the extensibility of it is extremely large with an elongation at break of nearly 3000%. This will provide new strategies for the development of tough plastics.

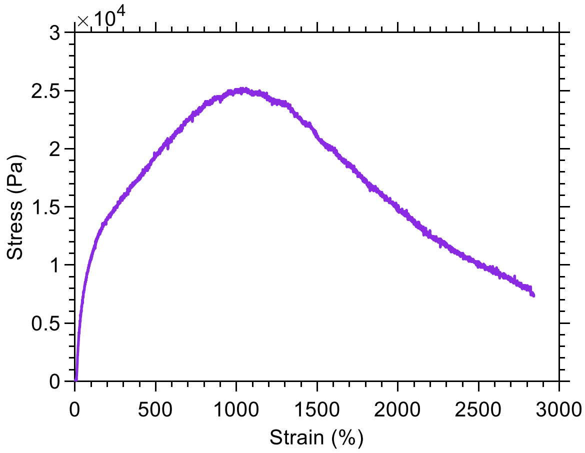

Figure 3.14 Stress-strain curve of LhBBL copolymer with x=2.15

3.4 Summary and potential work

This research designs a new polymer system based on linear-*hybrid* bottlebrush-linear (LhBBL) triblock copolymer, in which the end blocks are a linear polymer of relatively a high glass transition temperature T_g (BnMA), whereas the middle block is copolymerized with brush macromonomers of relatively a low T_g (PDMS) and small spacer monomers of a high T_g (BnMA). In this copolymer, two neighboring side chains are spaced by a short linear polymer segment which results in a *hybrid* bottlebrush consisting of both low and high T_g polymers. Through a well-designed synthetic routes via ARGET ATRP, a set of LhBBL copolymers with precisely controlled chemical parameters. The number of side-chain per middle block and number of monomer per end chain are keeping as constant, while only the number of spacer monomers along the backbone varies. Tensile test is performed using these samples and stress-strain curve of the samples shows an independently control of stiffness and extensibility. The Young’s modulus remain stable while the elongation at break increases exponentially with spacer/side-chain ratio. This phenomenon break through the traditional idea on the intrinsic relation between stiffness and extensibility of polymer network. This study would potentially establish a new design concept for mechanical materials and provide the important design parameters to create highly mechanically responsive materials. In application wise, such mechanical property will lead this new polymer system to potential applications in coatings, electronics, environmental sensing, and biomimetic engineering.

However, there still remains many aspects to be further studied. For instant, this work only investigates the dependence of mechanical behavior on spacer/side-chain ratio, the influence of weight fraction of end blocks, as well as the number of side-chains are necessary to be investigated. Furthermore, the microstructure of LhBBL copolymer has not been well studied. The insight view of the microstructure will provide a better understanding on the mechanism of decoupling the stiffness and extensibility of polymer network. Also, the generalization of concept that independently control over stiffness and extensibility of elastomer still needs to be further testified using other monomer systems.

Reference

1. Gent, A. N. I Rubber Elasticity: Basic Concepts and Behavior. 27.
2. Rubinstein, M. & Panyukov, S. Elasticity of Polymer Networks. *Macromolecules* **35**, 6670–6686 (2002).
3. Rubinstein, M. *Polymer physics*. (Oxford University, 2003).
4. Gent, A. N. Forms for the stored (strain) energy function for vulcanized rubber. *Journal of Polymer Science* **28**, 625–628.
5. Staverman, A.J., Properties of phantom networks and real networks, 1982. (Polymer Networks), K. Dušek, Editor, Springer Berlin Heidelberg: Berlin, Heidelberg. p. 73-101.
6. Heinrich, G., G. Helmis & E. Straube. Rubber elasticity of polymer networks: Theories. *Polymer physics* 33–87 (1988).
7. Valentín, J. L., Carretero-González, J., Mora-Barrantes, I., Chassé, W. & Saalwächter, K. Uncertainties in the Determination of Cross-Link Density by Equilibrium Swelling Experiments in Natural Rubber. *Macromolecules* **41**, 4717–4729 (2008).
8. Flory, P. J. & Erman, B. Theory of elasticity of polymer networks. 3. *Macromolecules* **15**, 800–806 (1982).
9. Chern, C.-S., Applications of Emulsion Polymers, 2008. (Principles and Applications of Emulsion Polymerization), John Wiley & Sons, Inc. p. 223-247.
10. Peterlin, A., The Physics of Glassy Polymers, R. N. Haward, Ed., Halsted Press, New York, 1973. 620 pp. $45.00. Journal of Polymer Science: Polymer Letters Edition, 1973. 11(10): p. 655-655.
11. Sperling, L.H., Mechanical Behavior of Polymers, 2005. (Introduction to Physical Polymer Science), John Wiley & Sons, Inc. p. 557-612.
12. Glover, J. D., McLaughlin, C. E., McFarland, M. K. & Pham, J. T. Extracting uncrosslinked material from low modulus sylgard 184 and the effect on mechanical properties. *Journal of Polymer Science* **58**, 343–351 (2020).
13. Cai, L.-H. Molecular understanding for large deformations of soft bottlebrush polymer networks. *Soft Matter* **16**, 6259–6264 (2020).
14. Nian, S. *et al.* Three-Dimensional Printable, Extremely Soft, Stretchable, and Reversible Elastomers from Molecular Architecture-Directed Assembly. *Chem. Mater.* **33**, 2436–2445 (2021).
15. Bosq, N., Guigo, N., Persello, J. & Sbirrazzuoli, N. Melt and glass crystallization of PDMS and PDMS silica nanocomposites. *Phys. Chem. Chem. Phys.* **16**, 7830–7840 (2014).
16. Semsarzadeh, M. A. & Ghahramani, M. The effect of poly(alkyl (meth)acrylate) segments on the thermodynamic properties, morphology and gas permeation properties of poly(alkyl (meth)acrylate)-b-poly(dimethyl siloxane) triblock copolymer membranes. *Journal of Membrane Science* **594**, 117400 (2020).
17. Kaya, İ. & Pala, Ç. Y. Thermodynamics of poly(benzyl methacrylate)–probe interactions at different temperatures by using inverse gas chromatography. *Fluid Phase Equilibria* **374**, 63–69 (2014).
18. *Flory, Paul J. Principles of polymer chemistry. Cornell University Press, 1953.*
19. *Hiemenz, Paul C., and Timothy P. Lodge. Polymer chemistry. CRC press, 2007.*
20. *Stevens, Malcolm P. Polymer chemistry. Vol. 2. New York: Oxford university press, 1990.*
21. Kato, M., Kamigaito, M., Sawamoto, M. & Higashimura, T. Polymerization of Methyl Methacrylate with the Carbon Tetrachloride/Dichlorotris-

(triphenylphosphine)ruthenium(II)/Methylaluminum Bis(2,6-di-tert-butylphenoxide) Initiating System: Possibility of Living Radical Polymerization. *Macromolecules* **28**, 1721–1723 (1995).
22. Wang, J.-S. & Matyjaszewski, K. Controlled/"living" radical polymerization. atom transfer radical polymerization in the presence of transition-metal complexes. *J. Am. Chem. Soc.* **117**, 5614–5615 (1995).
23. Georges, M. K., Veregin, R. P. N., Kazmaier, P. M. & Hamer, G. K. Narrow molecular weight resins by a free-radical polymerization process. *Macromolecules* **26**, 2987–2988 (1993).
24. Mayadunne, R. T. A. *et al.* Living Radical Polymerization with Reversible Addition−Fragmentation Chain Transfer (RAFT Polymerization) Using Dithiocarbamates as Chain Transfer Agents. *Macromolecules* **32**, 6977–6980 (1999).
25. Matyjaszewski, K. & Xia, J. Atom Transfer Radical Polymerization. *Chem. Rev.* **101**, 2921–2990 (2001).
26. Ouchi, M., Terashima, T. & Sawamoto, M. Transition Metal-Catalyzed Living Radical Polymerization: Toward Perfection in Catalysis and Precision Polymer Synthesis. *Chem. Rev.* **109**, 4963–5050 (2009).
27. Matyjaszewski, K. Atom Transfer Radical Polymerization (ATRP): Current Status and Future Perspectives. *Macromolecules* **45**, 4015–4039 (2012).
28. Fischer, H. The Persistent Radical Effect: A Principle for Selective Radical Reactions and Living Radical Polymerizations. *Chem. Rev.* **101**, 3581–3610 (2001).
29. Matyjaszewski, K., Jo, S. M., Paik, H. & Shipp, D. A. An Investigation into the CuX/2,2‘-Bipyridine (X = Br or Cl) Mediated Atom Transfer Radical Polymerization of Acrylonitrile. *Macromolecules* **32**, 6431–6438 (1999).
30. Teodorescu, M. & Matyjaszewski, K. Atom Transfer Radical Polymerization of (Meth)acrylamides. *Macromolecules* **32**, 4826–4831 (1999).
31. Zhang, Y., Wang, Y. & Matyjaszewski, K. ATRP of Methyl Acrylate with Metallic Zinc, Magnesium, and Iron as Reducing Agents and Supplemental Activators. *Macromolecules* **44**, 683–685 (2011).
32. Braunecker, W. A.; Matyjaszewski, K. Prog. Polym. Sci. 2007, 32, 93- 146.
33. Matyjaszewski, K.; Xia, J. Chem. Rev. 2001, 101, 2921-2990.
34. Wang, B.; Zhuang, Y.; Luo, X.; Xu, S.; Zhou, X. Macromolecules 2003, 36, 9684-9686.
35. Tang, W. *et al.* Understanding Atom Transfer Radical Polymerization: Effect of Ligand and Initiator Structures on the Equilibrium Constants. *J. Am. Chem. Soc.* **130**, 10702–10713 (2008).
36. Krys, P.; Matyjaszewski, K., Kinetics of Atom Transfer Radical Polymerization. Eur Polym J 2017, 89, 482-523.
37. Matyjaszewski, K. *et al.* Diminishing catalyst concentration in atom transfer radical polymerization with reducing agents. *Proceedings of the National Academy of Sciences* **103**, 15309–15314 (2006).
38. Bortolamei, N., Isse, A. A., Magenau, A. J. D., Gennaro, A. & Matyjaszewski, K. Controlled Aqueous Atom Transfer Radical Polymerization with Electrochemical Generation of the Active Catalyst. *Angew. Chem. Int. Ed.* **50**, 11391–11394 (2011).
39. Matyjaszewski, K. *et al.* Role of Cu ^{0} in Controlled/“Living” Radical Polymerization. *Macromolecules* **40**, 7795–7806 (2007).
40. Konkolewicz, D., Schröder, K., Buback, J., Bernhard, S. & Matyjaszewski, K. Visible Light and Sunlight Photoinduced ATRP with ppm of Cu Catalyst. *ACS Macro Lett.* **1**, 1219–1223 (2012).

41. Treat, N. J.; Sprafke, H.; Kramer, J. W.; Clark, P. G.; Barton, B. E.; de Alaniz, J. R.; Fors, B. P.; Hawker, C. J., Metal-Free Atom Transfer Radical Polymerization. J Am Chem Soc 2014, 136 (45), 16096-16101.
42. Pan, X. C.; Tasdelen, M. A.; Laun, J.; Junkers, T.; Yagci, Y.; Matyjaszewski, K., Photomediated Controlled Radical Polymerization. Prog Polym Sci 2016, 62, 73-125.
43. Chantasirichot, S.; Inoue, Y.; Ishihara, K., Photoinduced atom transfer radical polymerization in a polar solvent to synthesize a water-soluble poly(2-methacryloyloxyethyl phosphorylcholine) and its block-type copolymers. Polymer 2015,61, 55-60.

Supporting information

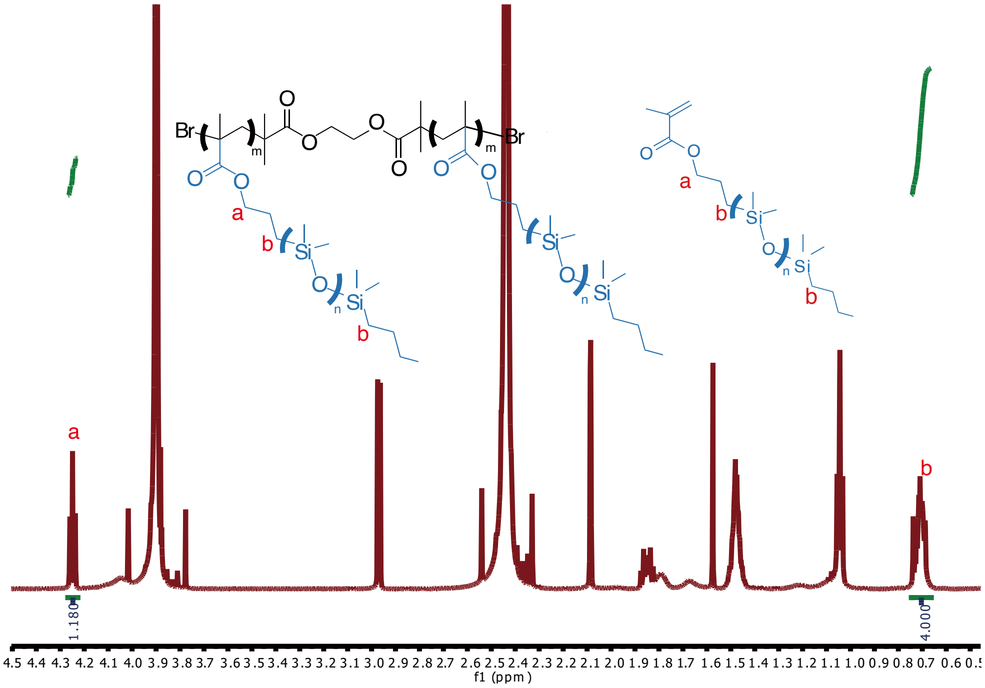

Figure S1. ^{1}H NMR spectrum of raw mixture of ARGET ATRP of poly(PDMS)$_{205}$ (CDCl$_3$, 25°C). $Conversion = (1 - Area(a) \times 2/Area(b)) \times 100\% = 41\%$. The polymer synthesized is bbPDMS with side chain 1kDa and DP of 205.

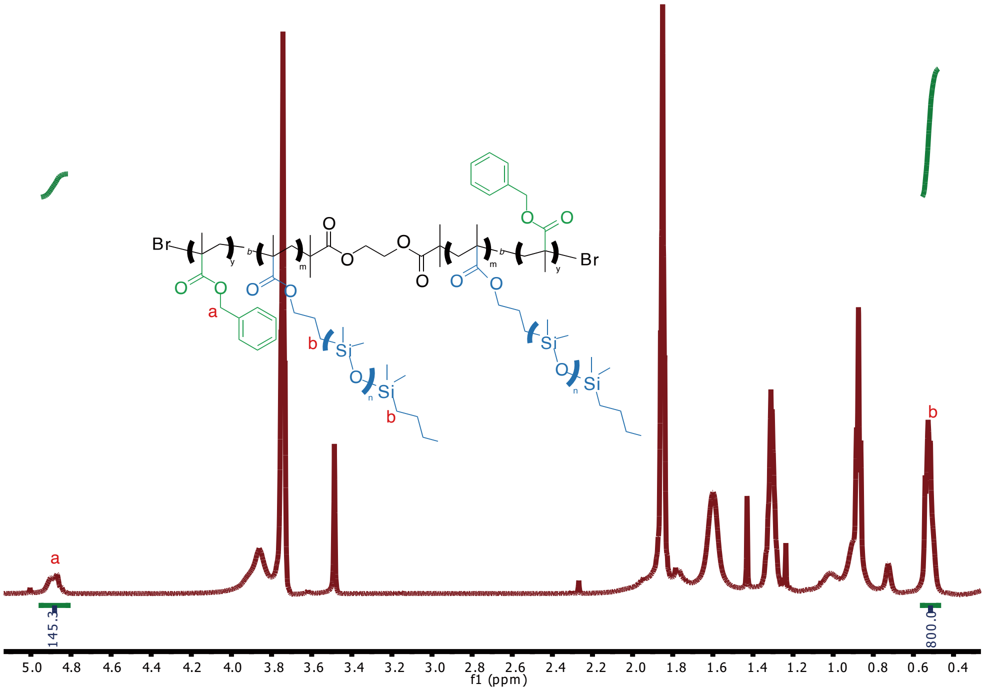

Figure S2. ^{1}H NMR spectrum of PBnMA$_{36}$-*b*-bbPDMS-*b*-BnMA$_{36}$ (CDCl$_3$, 25°C). $DP\ of\ each\ BnMA\ end\ block = DP\ of\ middle\ block \times Area(a)/Area(b) = 36$. Weight fraction of total PBnMA is around 5.8%.

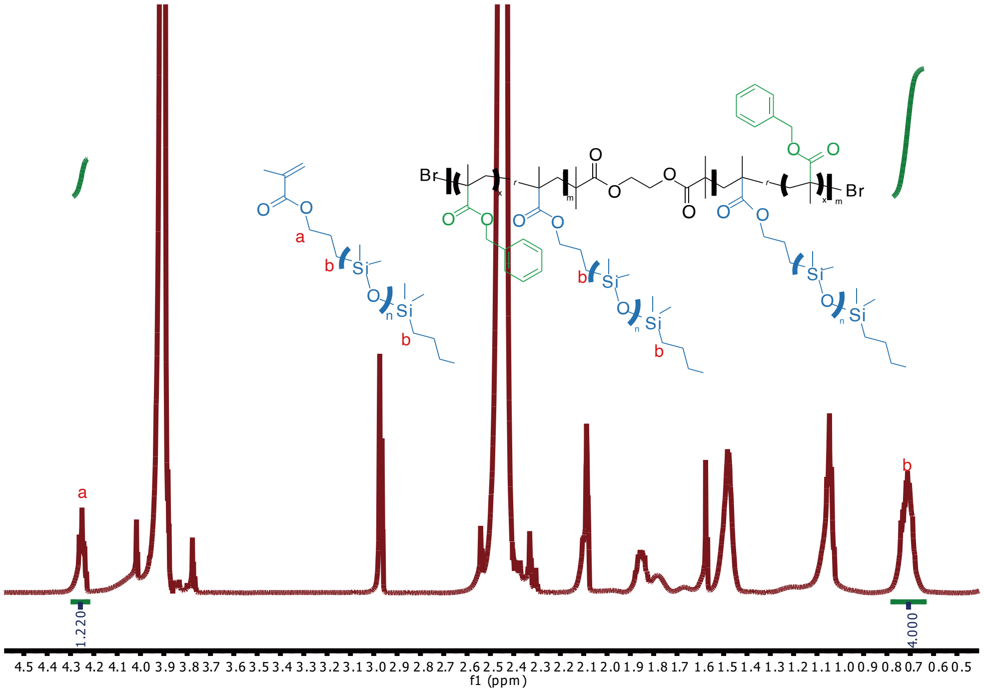

Figure S3. ^{1}H NMR spectrum of raw mixture of ARGET ATRP of poly(BnMA$_{0.31}$-*r*-PDMS)$_{195}$ (CDCl$_3$, 25°C). $Conversion\ rate\ of\ PDMS\ side\ chain = (1 - Area(a) \times 2/Area(b)) \times 100\% = 39\%$. DP of PDMS side chain is 195.

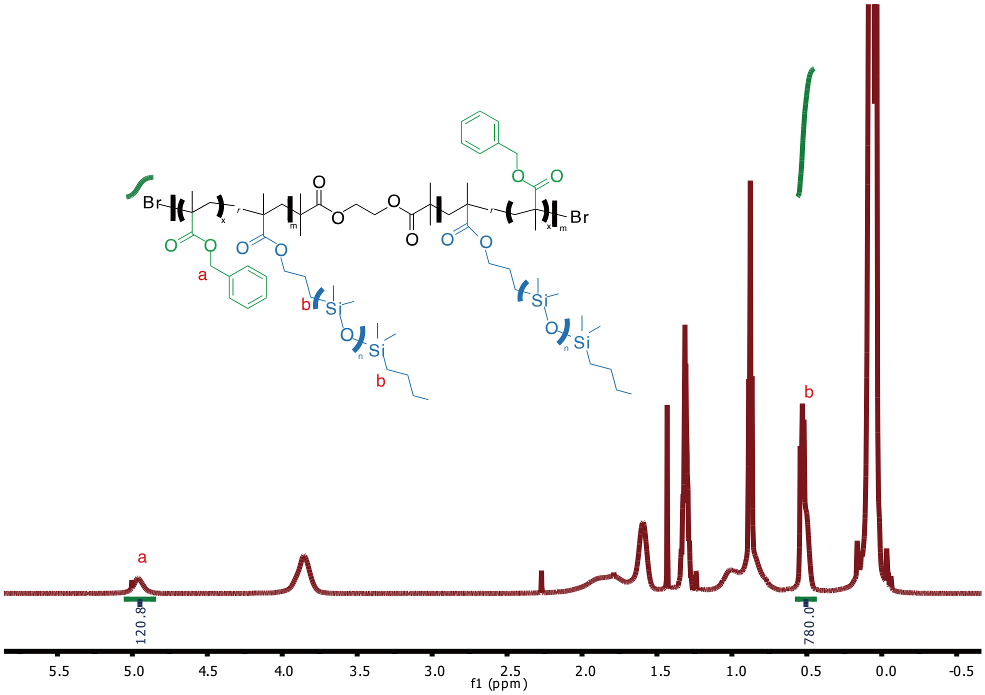

Figure S4. ^{1}H NMR spectrum of poly(BnMA$_{0.31}$-*r*-PDMS)$_{195}$ (CDCl$_3$, 25°C). $DP\ of\ spacers = DP\ of\ middle\ block \times Area(a) \times 2/Area(b) = 60$. Spacer/side chain ratio, x, is 0.31.

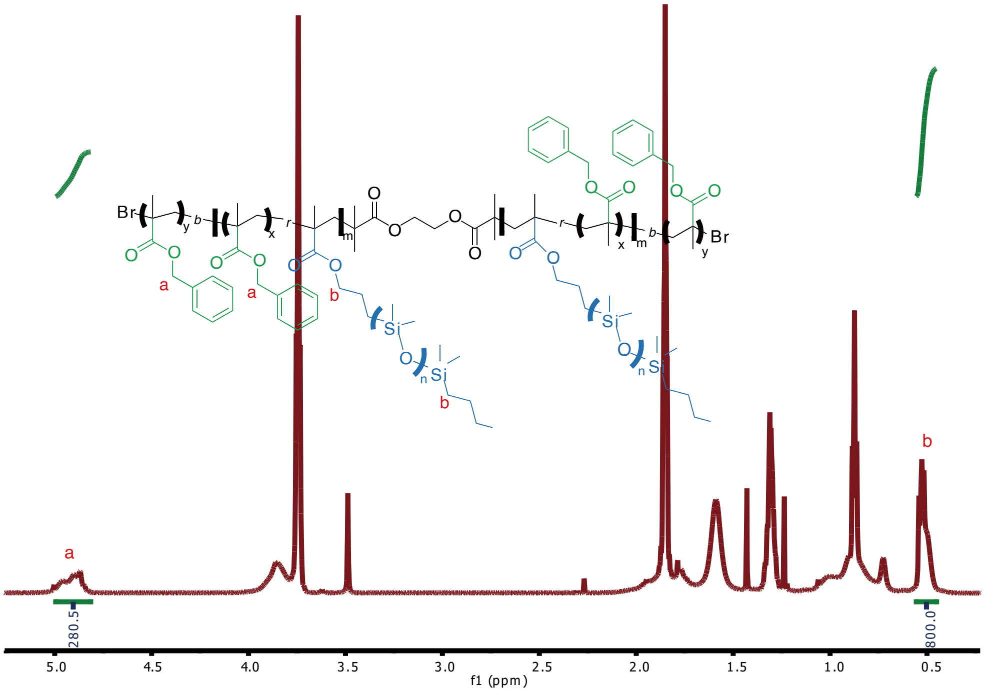

Figure S5. ^{1}H NMR spectrum of BnMA$_{40}$-*b*-(BnMA$_{0.31}$-*r*-PDMS)$_{195}$-*b*-BnMA$_{40}$ (CDCl$_3$, 25°C). $DP\ of\ each\ BnMA\ end\ block = (DP\ of\ sidechain \times 2 \times \frac{Area(a)}{Area(b)} - DP\ of\ spacer)/2 = 40$. Weight fraction of end chains to side-chains is around 6.7%.

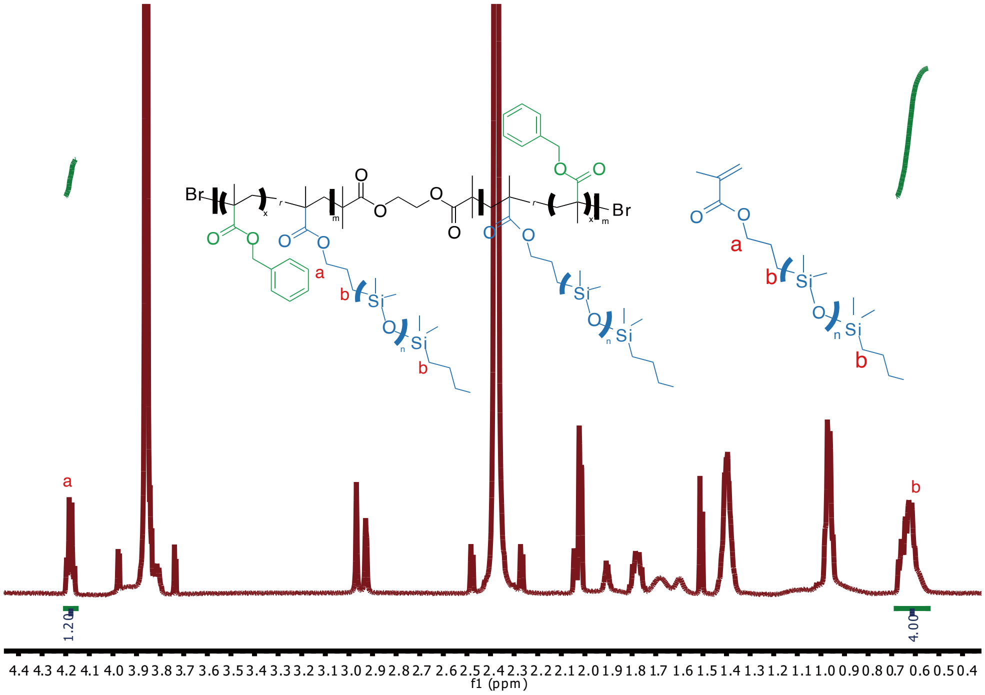

Figure S6. ^{1}H NMR spectrum of raw mixture of ARGET ATRP of poly(BnMA$_{0.60}$-*r*-PDMS)$_{200}$ (CDCl$_3$, 25°C). $Conversion\ rate\ of\ PDMS\ side\ chain = (1 - Area(a) \times 2/Area(b)) \times 100\% = 40\%$. DP of PDMS side chain is 200.

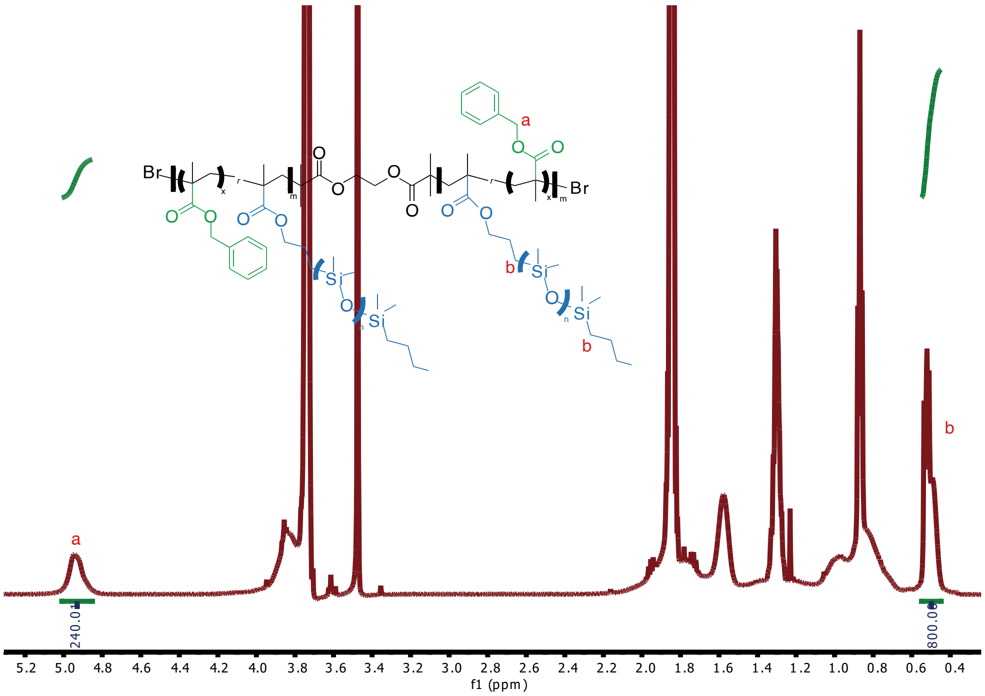

Figure S7. ^{1}H NMR spectrum of poly(BnMA$_{0.60}$-*r*-PDMS)$_{200}$ (CDCl$_3$, 25°C). $DP\ of\ spacers = DP\ of\ middle\ block \times Area(a) \times 2/Area(b) = 120$. Spacer/side chain ratio, *x*, is 0.60.

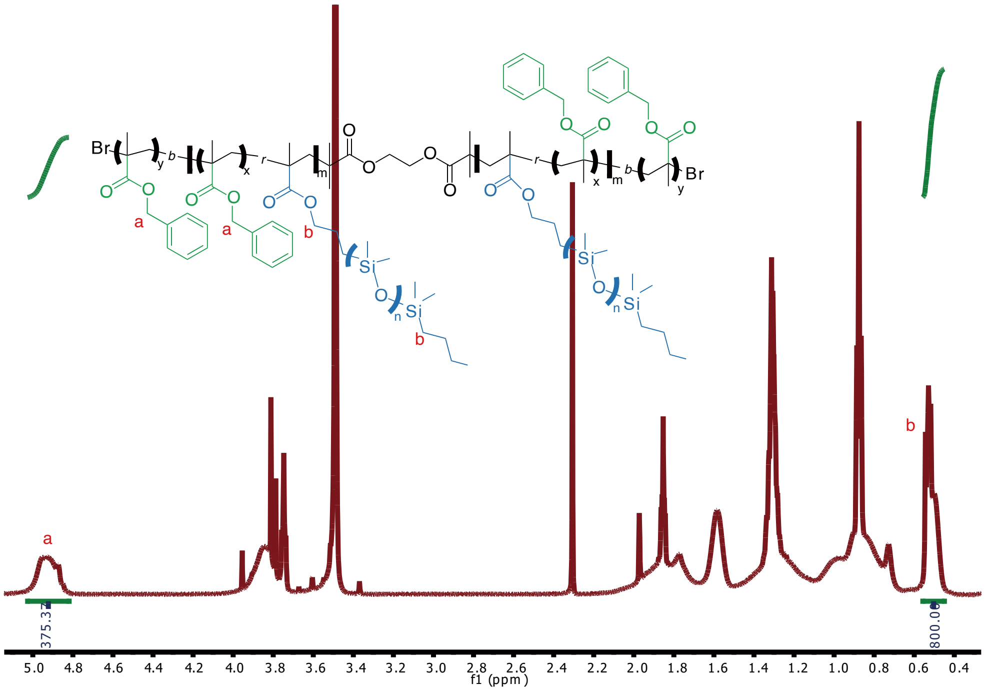

Figure S8. ^{1}H NMR spectrum of BnMA$_{33}$-b-(BnMA$_{0.60}$-r-PDMS)$_{200}$-b-BnMA$_{33}$ (CDCl$_3$, 25°C). $DP\ of\ each\ BnMA\ end\ block = (DP\ of\ sidechain \times 2 \times \frac{Area(a)}{Area(b)} - DP\ of\ spacer)/2 = 33$. Weight fraction of end chains to side-chains is around 5.5%.

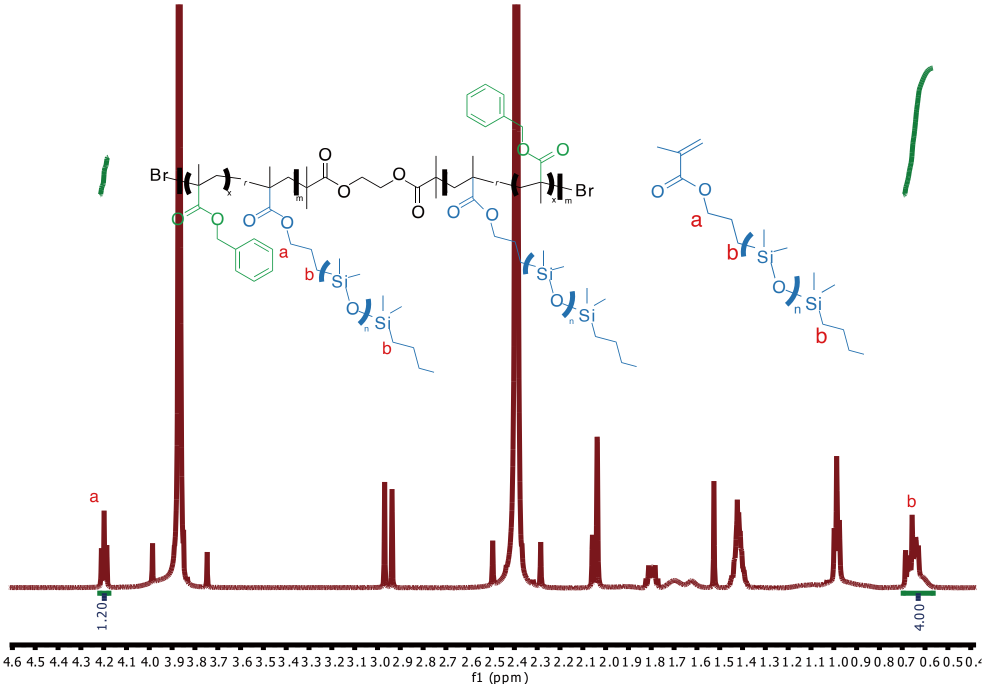

Figure S9. ^{1}H NMR spectrum of raw mixture of ARGET ATRP of poly(BnMA$_{0.83}$-r-PDMS)$_{200}$ (CDCl$_3$, 25°C). $Conversion\ rate\ of\ PDMS\ side\ chain = (1 - Area(a) \times 2/Area(b)) \times 100\% = 40\%$. DP of PDMS side chain is 200.

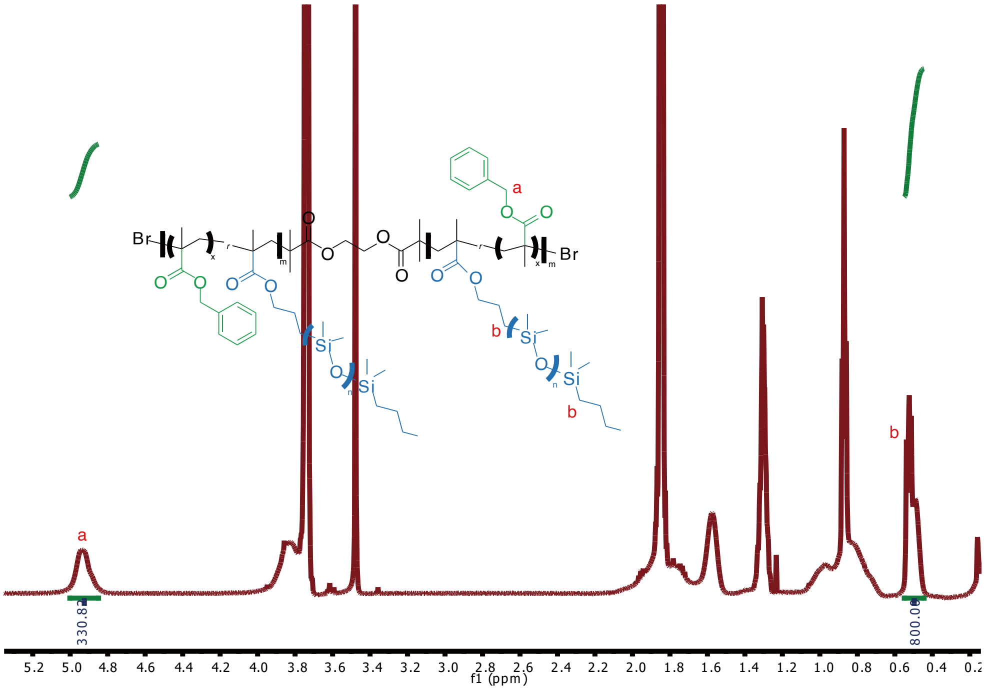

Figure S10. ^{1}H NMR spectrum of poly(BnMA$_{0.83}$-*r*-PDMS)$_{200}$ (CDCl$_3$, 25°C). $DP\ of\ spacers = DP\ of\ middle\ block \times Area(a) \times 2/Area(b) = 166$. Spacer/side chain ratio, *x*, is 0.83.

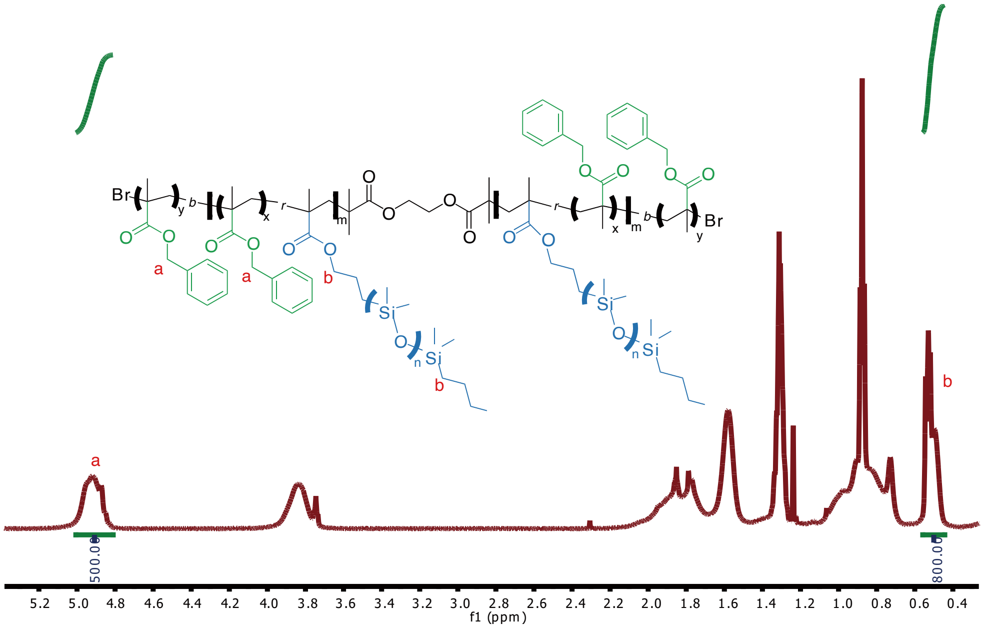

Figure S11. ^{1}H NMR spectrum of BnMA$_{42}$-*b*-(BnMA$_{0.83}$-*r*-PDMS)$_{200}$-*b*-BnMA$_{42}$ (CDCl$_3$, 25°C). $DP\ of\ each\ BnMA\ end\ block = (DP\ of\ sidechain \times 2 \times \frac{Area(a)}{Area(b)} - DP\ of\ spacer)/2 = 42$. fraction of end chains to side-chains is around 6.9%.

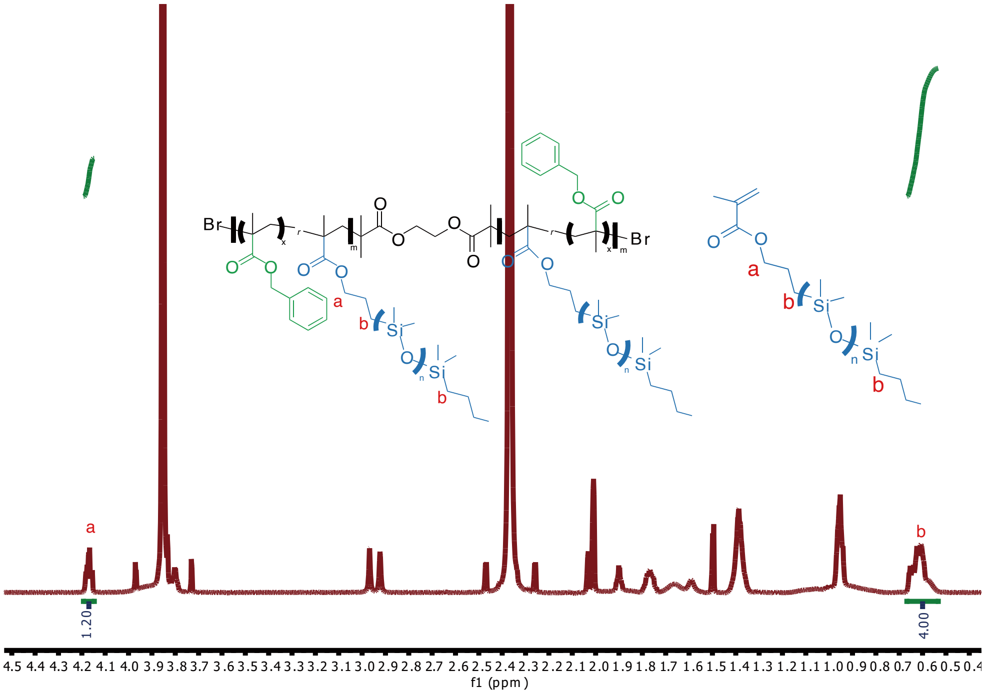

Figure S12. ^{1}H NMR spectrum of raw mixture of ARGET ATRP of poly(BnMA$_{0.88}$-*r*-PDMS)$_{200}$ (CDCl$_3$, 25°C). $Conversion\ rate\ of\ PDMS\ side\ chain = (1 - Area(a) \times 2/Area(b)) \times 100\% = 40\%$. DP of PDMS side chain is 200.

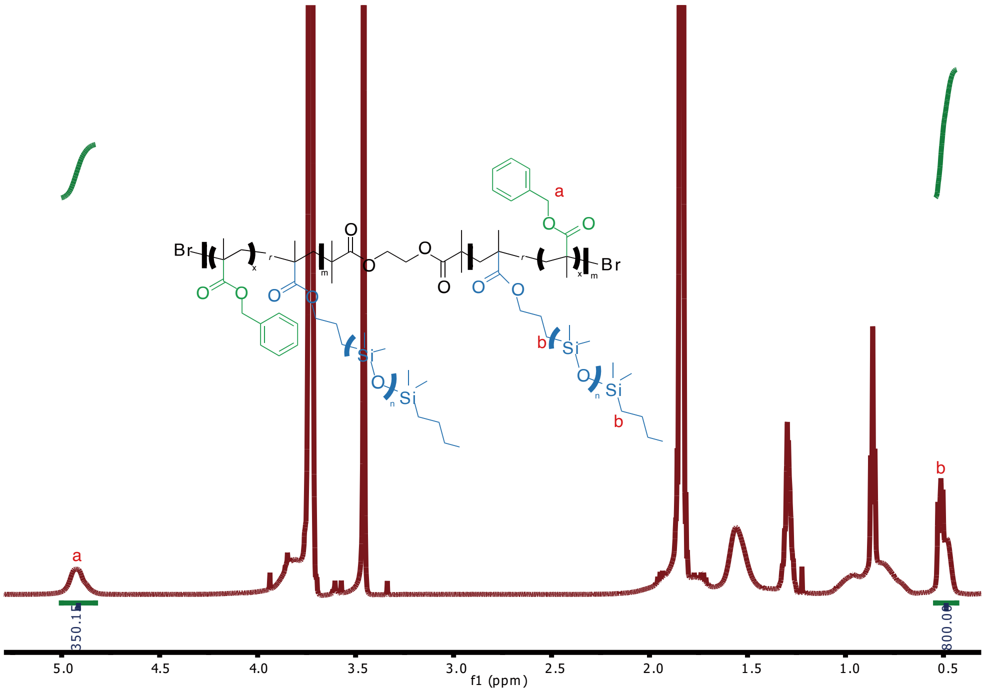

Figure S13. ^{1}H NMR spectrum of poly(BnMA$_{0.88}$-*r*-PDMS)$_{200}$ (CDCl$_3$, 25°C). $DP\ of\ spacers = DP\ of\ middle\ block \times Area(a) \times 2/Area(b) = 176$. Spacer/side chain ratio, *x*, is 0.88.

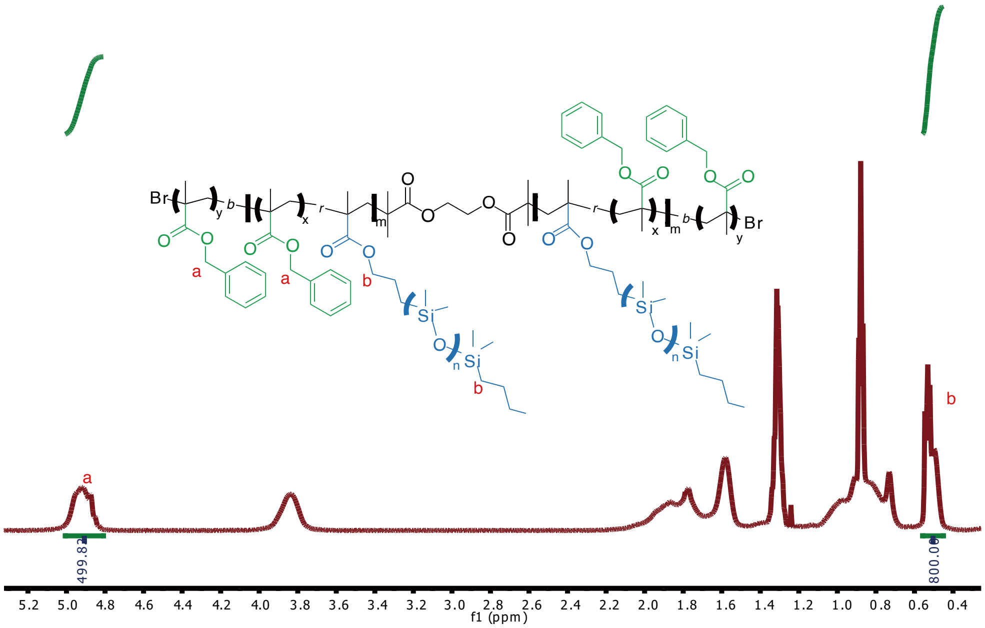

Figure S14. ^{1}H NMR spectrum of $BnMA_{34}$-*b*-($BnMA_{0.88}$-*r*-PDMS)$_{200}$-*b*-$BnMA_{34}$ ($CDCl_3$, 25°C). $DP\ of\ each\ BnMA\ end\ block = (DP\ of\ sidechain \times 2 \times \frac{Area(a)}{Area(b)} - DP\ of\ spacer)/2 = 34$. Weight fraction of end chains to side-chains is around 5.6%.

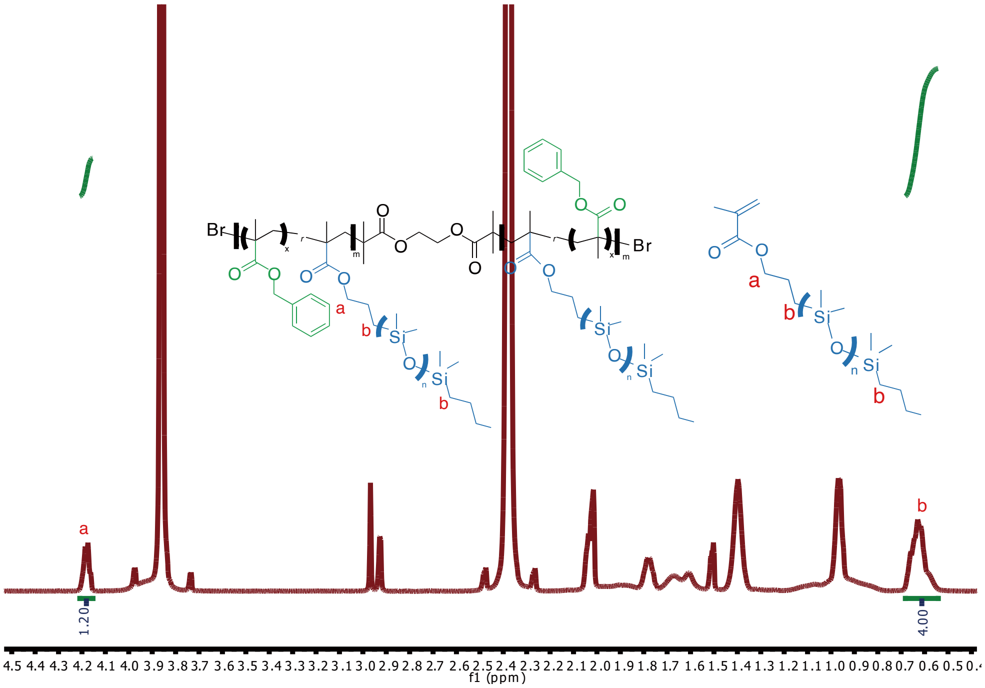

Figure S15. ^{1}H NMR spectrum of raw mixture of ARGET ATRP of poly($BnMA_{1.00}$-*r*-PDMS)$_{200}$ ($CDCl_3$, 25°C). $Conversion\ rate\ of\ PDMS\ side\ chain = (1 - Area(a) \times 2/Area(b)) \times 100\% = 40\%$. DP of PDMS side chain is 200.

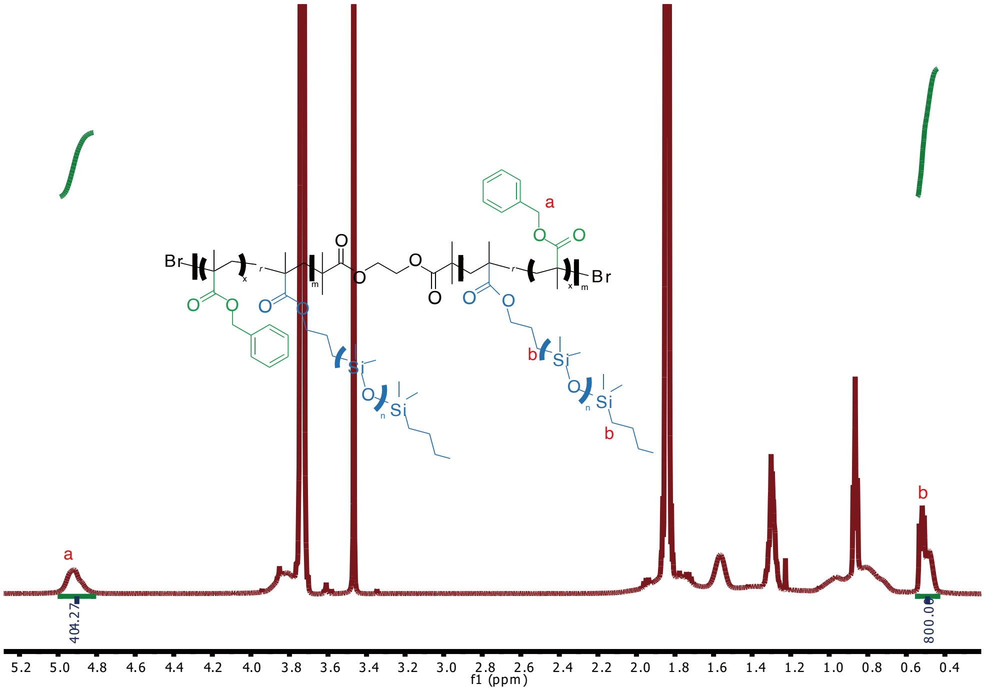

Figure S16. ^{1}H NMR spectrum of poly(BnMA$_{1.00}$-*r*-PDMS)$_{200}$ (CDCl$_3$, 25°C). $DP\ of\ spacers = DP\ of\ middle\ block \times Area(a) \times 2/Area(b) = 200$. Spacer/side chain ratio, *x*, is 1.00.

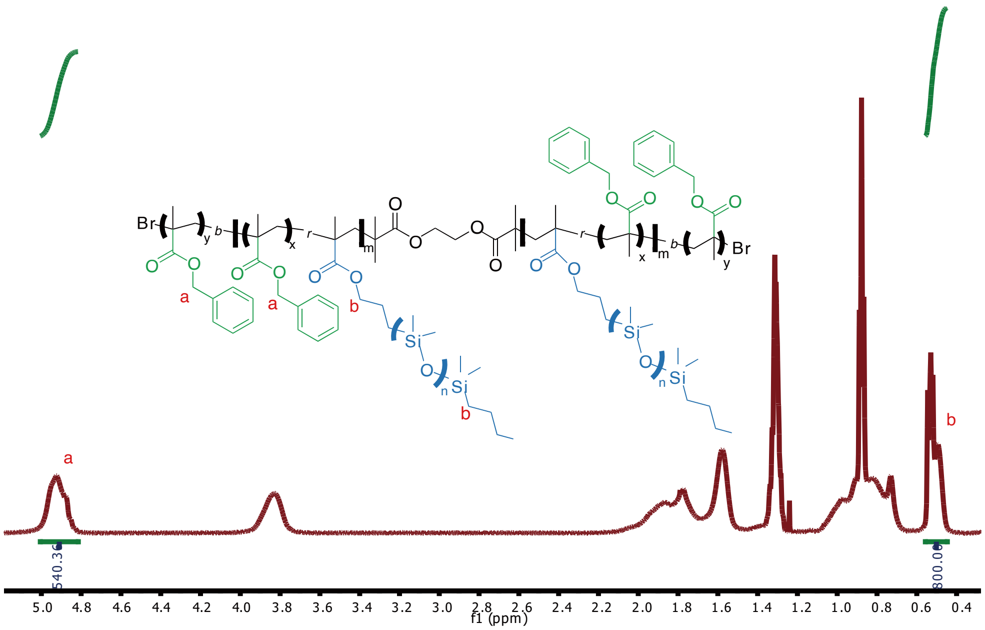

Figure S17. ^{1}H NMR spectrum of BnMA$_{33}$-*b*-(BnMA$_{1.00}$-*r*-PDMS)$_{195}$-*b*-BnMA$_{33}$ (CDCl$_3$, 25°C). $DP\ of\ each\ BnMA\ end\ block = (DP\ of\ sidechain \times 2 \times \frac{Area(a)}{Area(b)} - DP\ of\ spacer)/2 = 33$. Weight fraction of end chains to side-chains is around 5.5%.

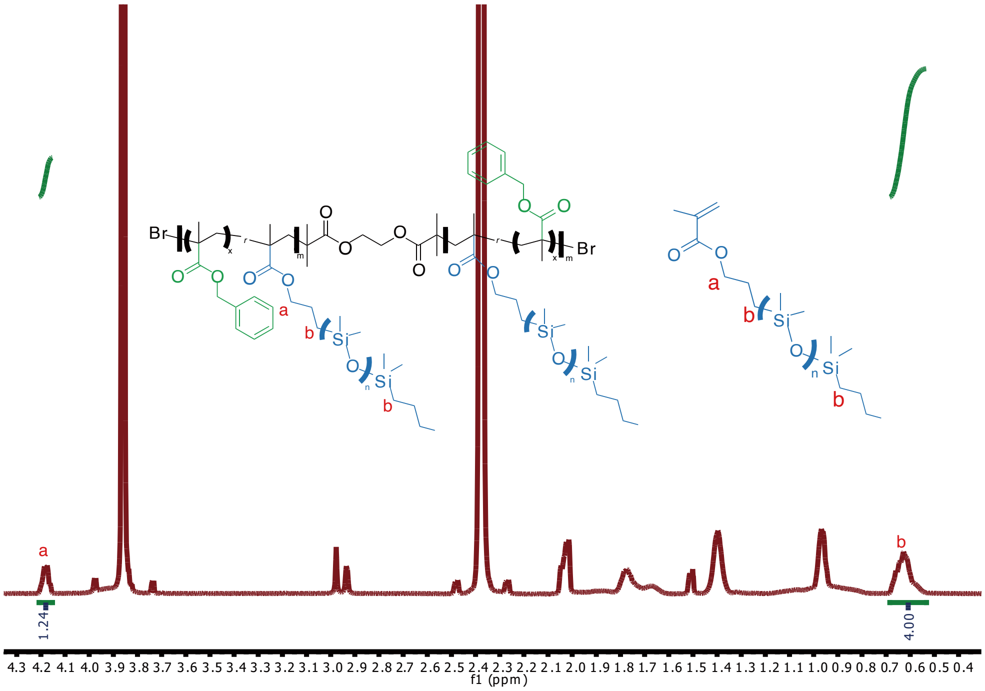

Figure S18. ^{1}H NMR spectrum of raw mixture of ARGET ATRP of poly(BnMA$_{1.26}$-*r*-PDMS)$_{190}$ (CDCl$_3$, 25°C). $Conversion\ rate\ of\ PDMS\ side\ chain = (1 - Area(a) \times 2/Area(b)) \times 100\% = 38\%$. DP of PDMS side chain is 190.

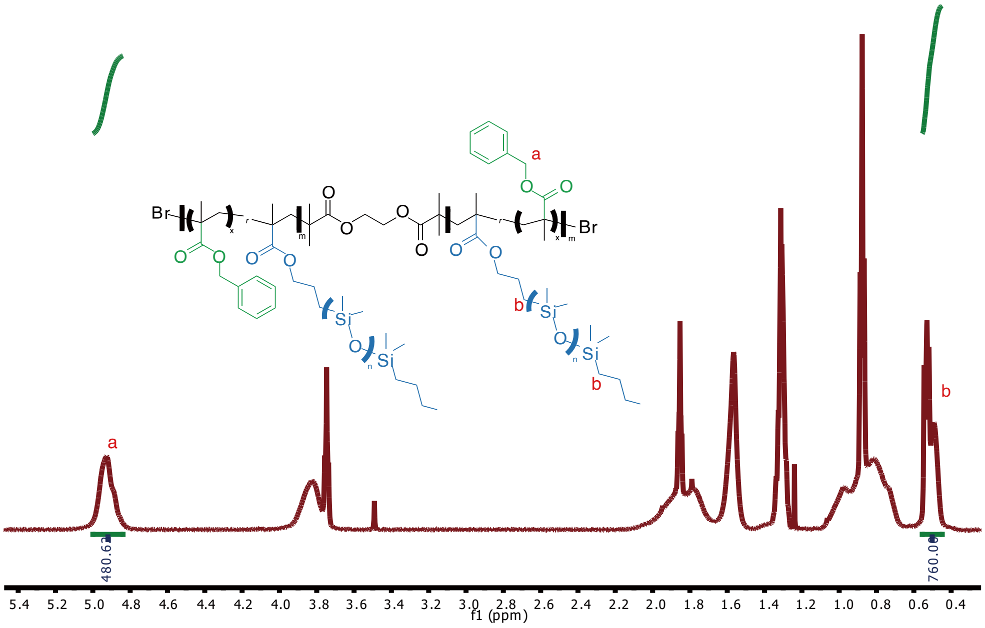

Figure S19. ^{1}H NMR spectrum of poly(BnMA$_{1.26}$-*r*-PDMS)$_{190}$ (CDCl$_3$, 25°C). $DP\ of\ spacers = DP\ of\ middle\ block \times Area(a) \times 2/Area(b) = 240$. Spacer/side chain ratio, *x*, is 1.26.

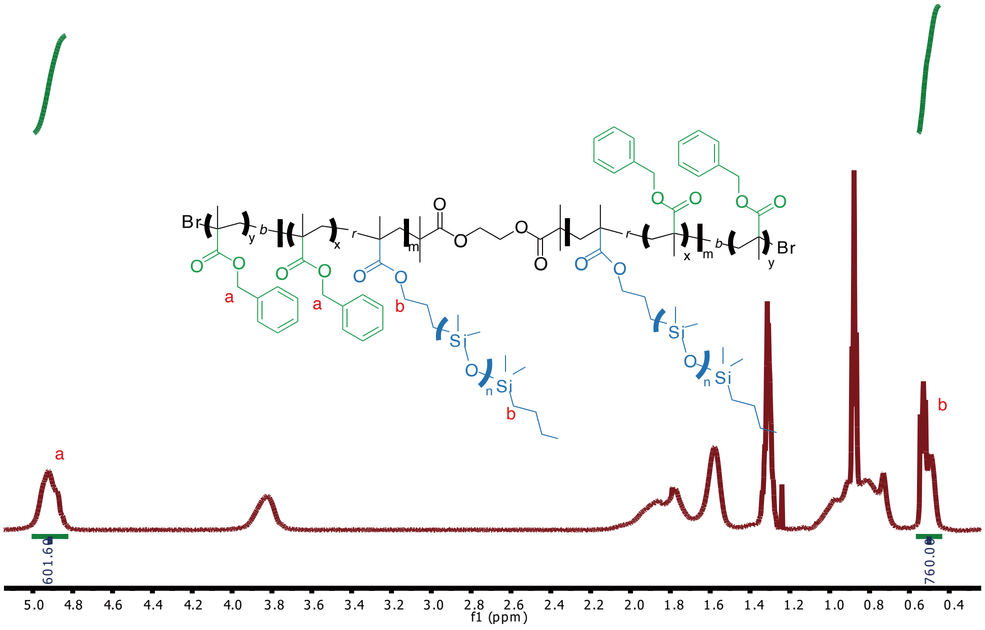

Figure S20. ^{1}H NMR spectrum of BnMA$_{30}$-*b*-(BnMA$_{1.26}$-*r*-PDMS)$_{190}$-*b*-BnMA$_{30}$ (CDCl$_3$, 25°C). $DP\ of\ each\ BnMA\ end\ block = (DP\ of\ sidechain \times 2 \times \frac{Area(a)}{Area(b)} - DP\ of\ spacer)/2 = 30$. Weight fraction of end chains to side-chains is around 5.3%.

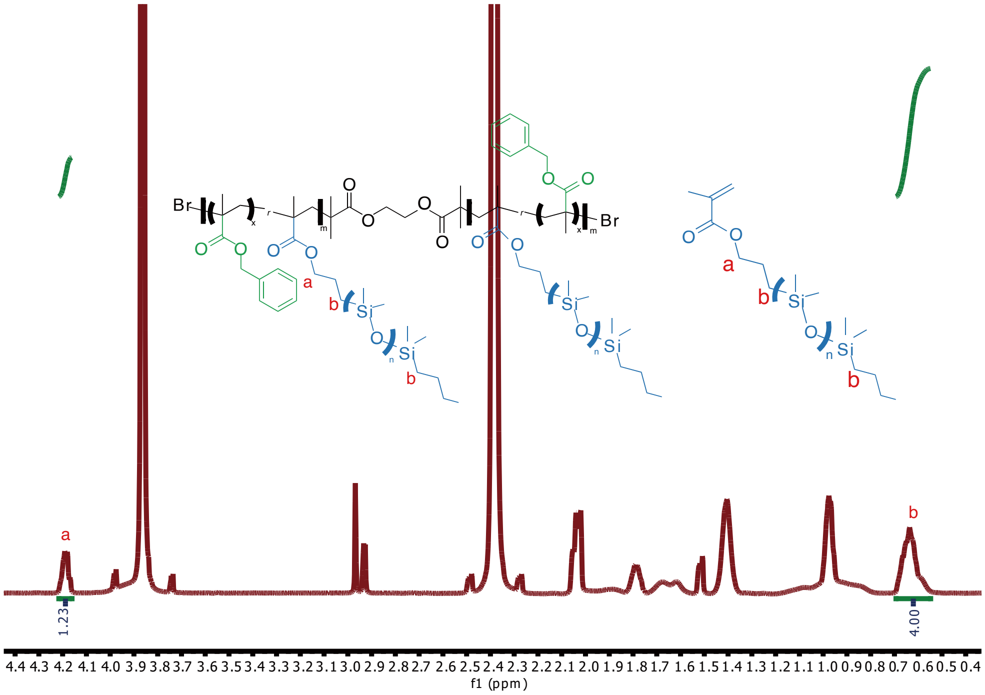

Figure S21. ^{1}H NMR spectrum of raw mixture of ARGET ATRP of poly(BnMA$_{1.42}$-r-PDMS)$_{190}$ (CDCl$_3$, 25°C). $Conversion\ rate\ of\ PDMS\ side\ chain = (1 - Area(a) \times 2/Area(b)) \times 100\% = 38\%$. DP of PDMS side chain is 190.

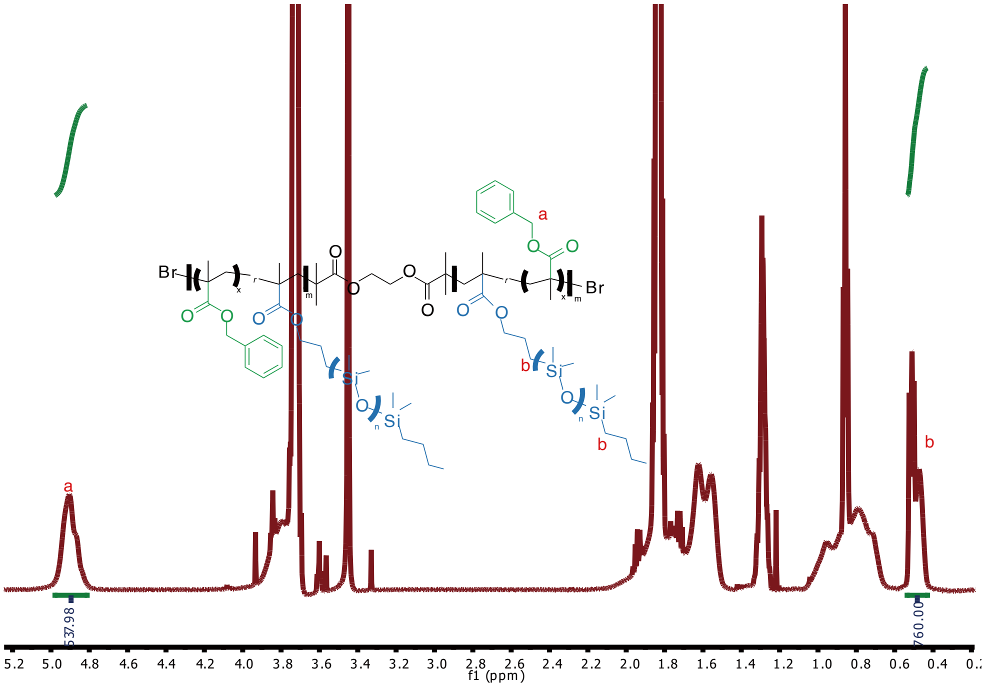

Figure S22. ^{1}H NMR spectrum of poly(BnMA$_{1.42}$-r-PDMS)$_{190}$ (CDCl$_3$, 25°C). $DP\ of\ spacers = DP\ of\ middle\ block \times Area(a) \times 2/Area(b) = 270$. Spacer/side chain ratio, x, is 1.42.

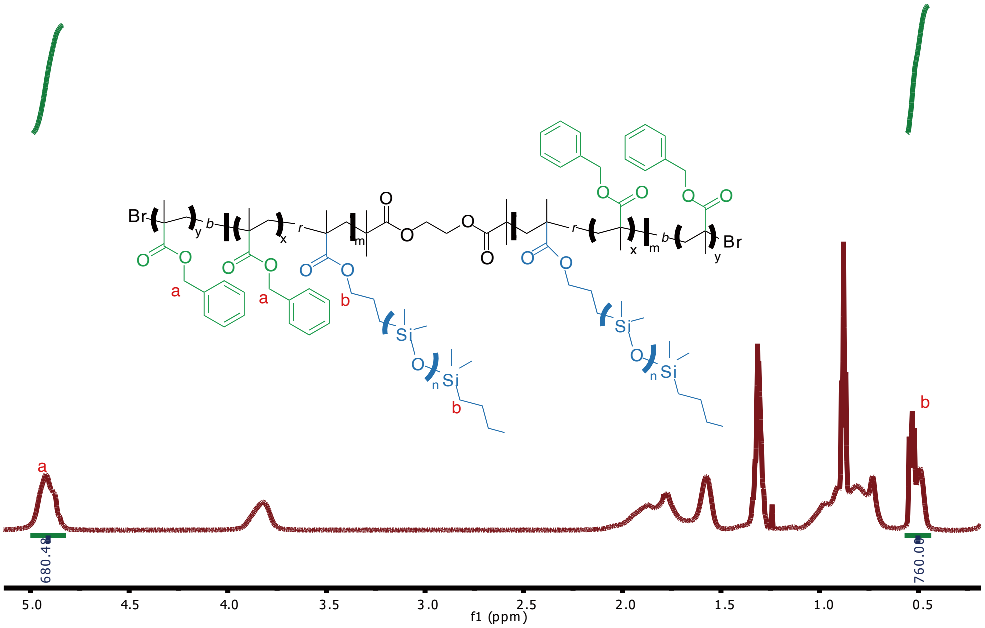

Figure S23. ^{1}H NMR spectrum of BnMA$_{31}$-*b*-(BnMA$_{1.42}$-*r*-PDMS)$_{190}$-*b*-BnMA$_{31}$ (CDCl$_3$, 25°C). $DP\ of\ each\ BnMA\ end\ block = (DP\ of\ sidechain \times 2 \times \frac{Area(a)}{Area(b)} - DP\ of\ spacer)/2 = 31$. Weight fraction of end chains to side-chains is around 3.4%.

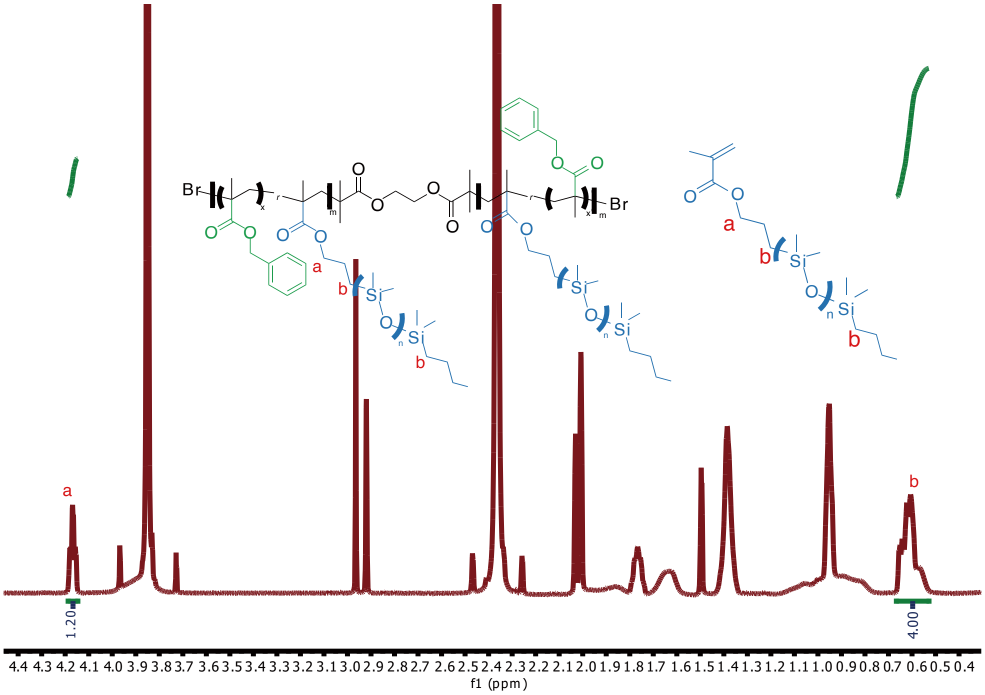

Figure S24. ^{1}H NMR spectrum of raw mixture of ARGET ATRP of poly(BnMA$_{1.48}$-*r*-PDMS)$_{200}$ (CDCl$_3$, 25°C). $Conversion\ rate\ of\ PDMS\ side\ chain = (1 - Area(a) \times 2/Area(b)) \times 100\% = 40\%$. DP of PDMS side chain is 200.

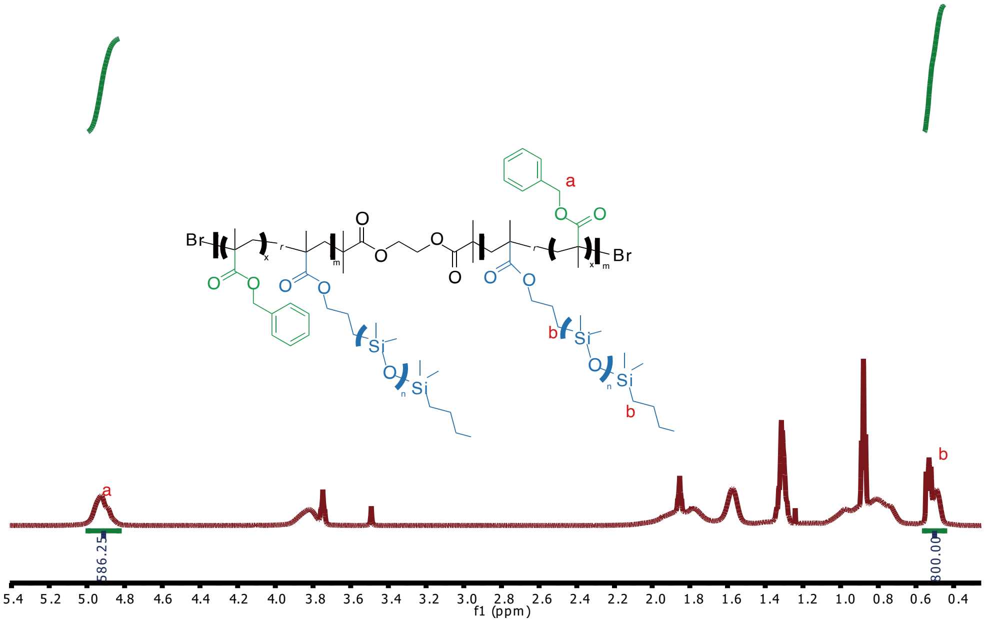

Figure S25. ^{1}H NMR spectrum of poly(BnMA$_{1.48}$-*r*-PDMS)$_{200}$ (CDCl$_3$, 25°C). $DP\ of\ spacers = DP\ of\ middle\ block \times Area(a) \times 2/Area(b) = 296$. Spacer/side chain ratio, *x*, is 1.48.

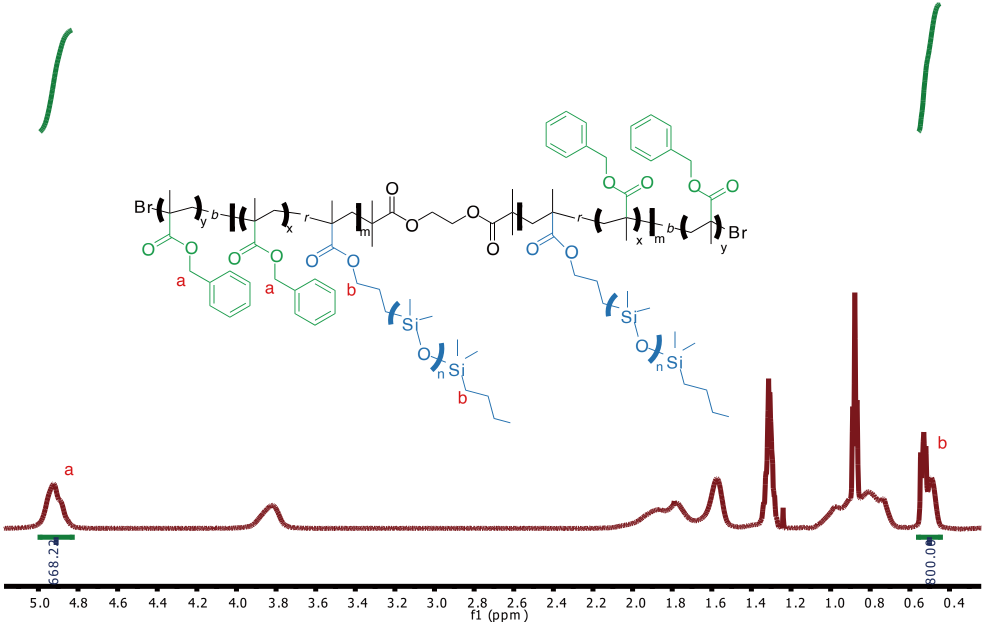

Figure S26. ^{1}H NMR spectrum of BnMA$_{20}$-*b*-(BnMA$_{1.48}$-*r*-PDMS)$_{200}$-*b*-BnMA$_{20}$ (CDCl$_3$, 25°C). $DP\ of\ each\ BnMA\ end\ block = (DP\ of\ sidechain \times 2 \times \frac{Area(a)}{Area(b)} - DP\ of\ spacer)/2 = 20$. Weight fraction of end chains to side-chains is around 3.4%.

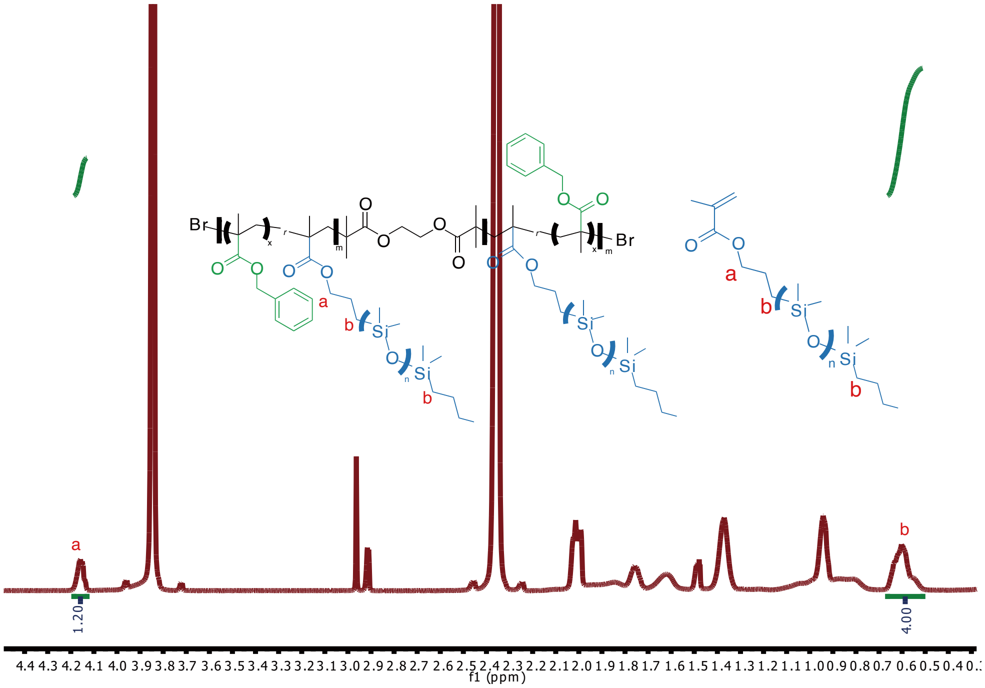

Figure S27. ^{1}H NMR spectrum of raw mixture of ARGET ATRP of poly(BnMA$_{2.15}$-*r*-PDMS)$_{200}$ (CDCl$_3$, 25°C). $Conversion\ rate\ of\ PDMS\ side\ chain = (1 - Area(a) \times 2/Area(b)) \times 100\% = 40\%$. DP of PDMS side chain is 200.

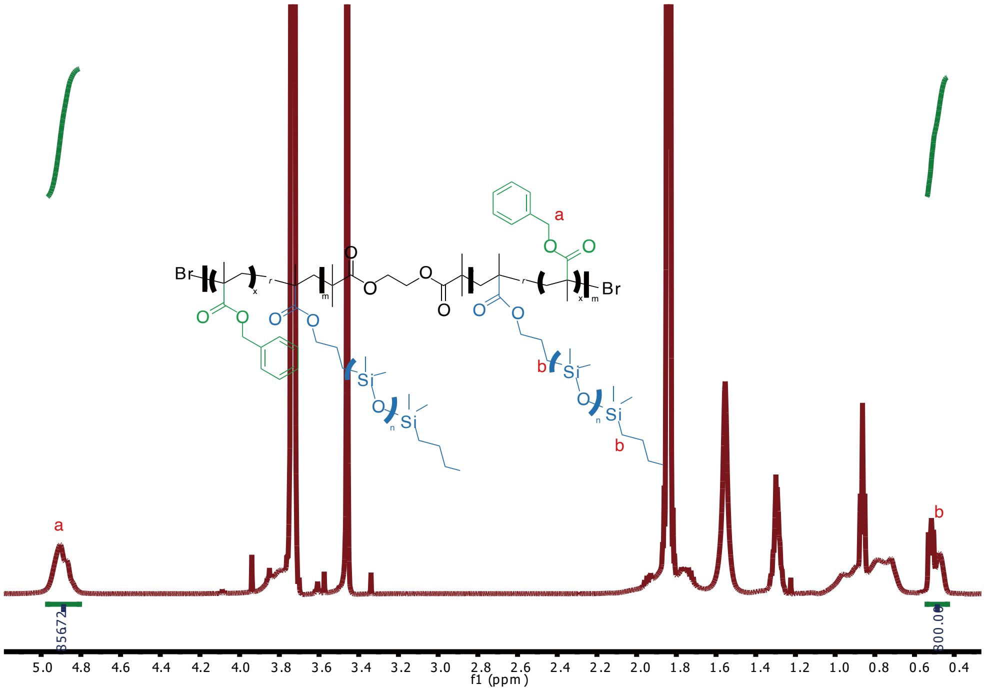

Figure S28. ^{1}H NMR spectrum of poly(BnMA$_{2.15}$-*r*-PDMS)$_{200}$ (CDCl$_3$, 25°C). $DP\ of\ spacers = DP\ of\ middle\ block \times Area(a) \times 2/Area(b) = 430$. Spacer/side chain ratio, *x*, is 2.15.

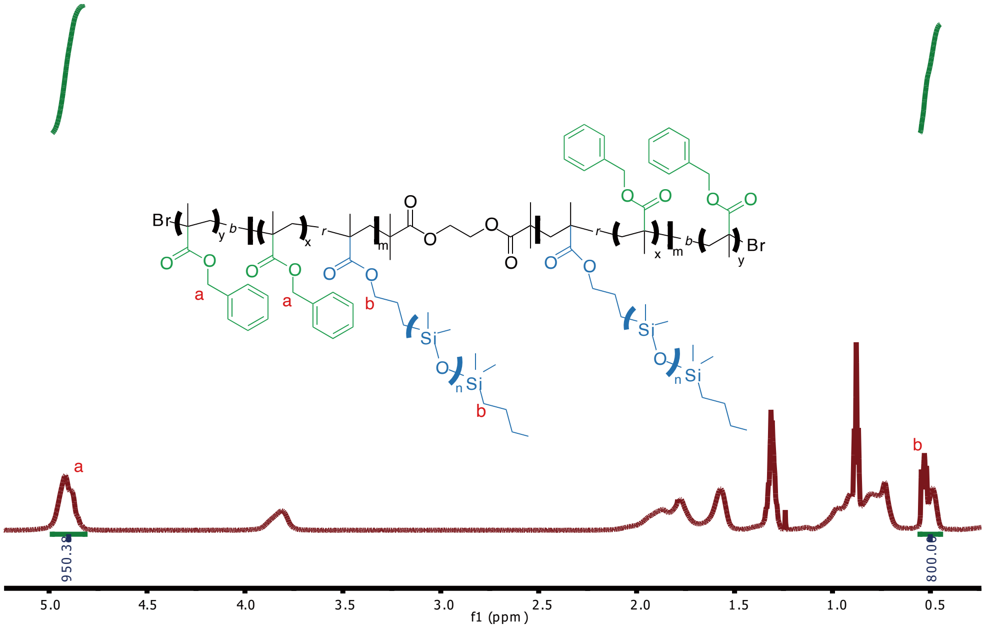

Figure S29. ^{1}H NMR spectrum of BnMA$_{23}$-*b*-(BnMA$_{2.15}$-*r*-PDMS)$_{200}$-*b*-BnMA$_{23}$ (CDCl$_3$, 25°C).

$$DP\ of\ each\ BnMA\ end\ block = (DP\ of\ sidechain \times 2 \times \frac{Area(a)}{Area(b)} - DP\ of\ spacer)/2 = 23 \quad .$$

Weight fraction of end chains to side-chains is around 3.9%.

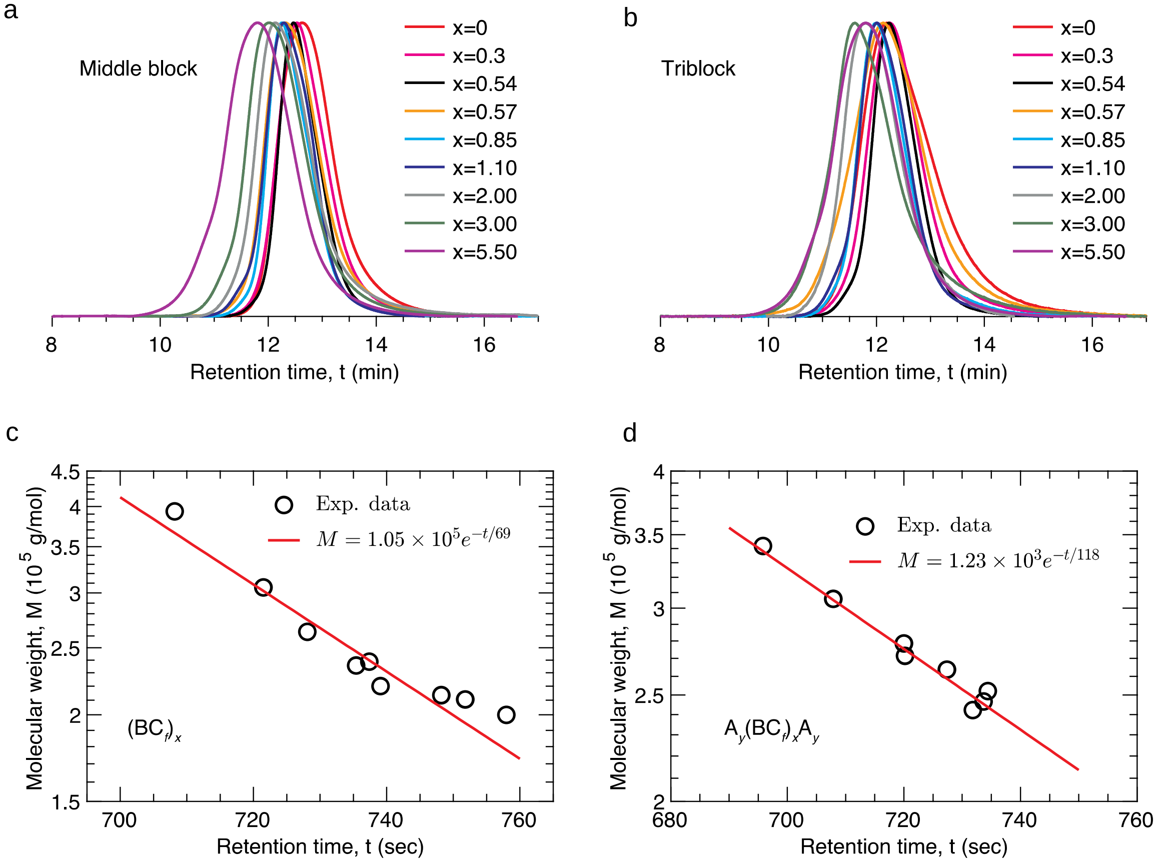

Figure S30. GPC data of LhBBL copolymers: (a) GPC curves for hybrid bottlebrush middle blocks. (b) GPC curves for LhBBL triblock copolymers. (c) Relationship between molecular weight of middle block to retention time. (d) Relationship between molecular weight of triblock copolymer to retention time.